Mitochondrial Genome Acquisition Restores Respiratory Function and Tumorigenic Potential of Cancer Cells Without Mitochondrial DNA

An S. Tan,[1,#] James W. Baty,[1,#] Lan-Feng Dong,[2,#] Ayenachew Bezawork-Geleta,[2] Berwini Endaya,[2] Jacob Goodwin,[2] Martina Bajzikova,[3] Jaromira Kovarova, [3] Martin Peterka,[3] Bing Yan,[2] Elham Alizadeh Pesdar,[2] Margarita Sobol,[4] Anatolyj Filimonenko,[4] Shani Stuart,[5] Magdalena Vondrusova,[3] Katarina Kluckova,[3] Karishma Sachaphibulkij,[2] Jakub Rohlena,[3] Pavel Hozak,[4] Jaroslav Truksa,[3] David Eccles[1], Larisa Haupt, [5] Lyn Griffiths,[5] Jiri Neuzil,[2,3,*] and Michael V. Berridge[1,*]

[1]Malaghan Institute of Medical Research, Victoria University, Wellington, 6012, New Zealand, [2]School of Medical Science, Griffith University, Southport, Qld, 4222 Australia, [3]Institute of Biotechnology, [4]Institute of Molecular Genetics, Academy of Sciences of the Czech Republic, Prague, 142 20 Czech Republic and Institute of Health and [5] Biomedical Innovation, Queensland University of Technology, Kelvin Grove, Qld, 4059 Australia.

[#]These authors contributed equally to the work.

Running title: Remodeling tumor respiration by mtDNA acquisition

[*]Correspondence: Michael V. Berridge, Cancer Cell and Molecular Biology Group, Malaghan Institute of Medical Research, Victoria University, Wellington, 6012, New Zealand; email mberridge@malaghan.org.nz; phone +64 4 499 6914 or Jiri Neuzil, Mitochondria, Apoptosis and Cancer Research Group, School of Medical Science and Griffith Health Institute, Griffith University, Gold Coast Campus, Southport, Qld 4222, Australia; email j.neuzil@griffith.edu.au: phone +61 7 55529109.

SUMMARY

We report that tumor cells devoid of their mitochondrial genome (mtDNA) show delayed tumor growth and that tumor formation is associated with acquisition of mtDNA from host cells. This leads to partial recovery of mitochondrial function in cells derived from primary tumors grown from cells without mtDNA and a shorter lag in tumor growth. Cell lines from circulating tumor cells showed further recovery of mitochondrial respiration and an intermediate lag to tumor growth, while cells from lung metastases exhibited full restoration of respiratory function and no lag in tumor growth. Stepwise assembly of mitochondrial respiratory supercomplexes was correlated with acquisition of respiratory function. Our findings indicate horizontal transfer of mtDNA from host cells in the tumor microenvironment to tumor cells with compromised respiratory function to re-establish respiration and tumor-initiating efficacy. These results suggest a novel pathophysiological process for overcoming mtDNA damage and support the notion of high plasticity of malignant cells.

INTRODUCTION

Mitochondria are structurally dynamic organelles with a circular genome (mtDNA) of ~16.5 kb in mammals, encoding 13 subunits of the respiratory complexes (RCs), 22 tRNAs and two rRNAs. Cells contain discreet and networked mitochondria, each with multiple mtDNA copies. The mitochondrial proteome comprises ~1,500 proteins, the vast majority of which are encoded by nuclear DNA (nDNA) (Neupert and Herrmann, 2007; Wallace, 2012). Of importance for the replication and transcription of mtDNA is the regulatory *D-LOOP*, which binds the mitochondrial transcription factor TFAM and other regulatory proteins (Falkenberg et al., 2007). A major role of mitochondria, generation of ATP, is facilitated by oxidative phosphorylation (OXPHOS) comprising four complexes of the electron transport chain (ETC), complex I (CI), CII, CIII and CIV, and CV with ATP synthase activity. RCs form supercomplexes (SCs), such as the respirasome (Schägger and Pfeiffer, 2010; Acin-Perez et al., 2008; Althoff et al., 2011) that transfers electrons from CI to CIV via CIII (Lapuente-Brun et al., 2013). RCs and SCs are assembled stepwise in a process involving specific factors (Moreno-Lastres et al., 2012; Lapuente-Brun et al., 2013; Ikeda et al., 2013).

Due to the central role of mitochondria in homeostasis, cells have conserved control systems to maintain mitochondrial integrity, appropriate mitochondrial mass, and bioenergetic and metabolic functions. In many pathologies, mtDNA mutations affect tissues with high demand for energy (Krishnan et al., 2008; Lu et al., 2009; Schon et al., 2012; Wallace, 2012). Cancer is characterized by altered energy metabolism (DeBarardinis et al 2007, Kroemer and Pouyssegur, 2008; Vander Heiden et al., 2009; Ralph et al., 2010; Hanahan and Weinberg, 2011) involving not only genetic alterations in nDNA, but also mtDNA mutations and changes in mtDNA copy number (Surani,

2001; Wallace and Fan, 2010; De Carvalho, 2010; Plass et al., 2013). Certain mtDNA mutations compromise ETC function and contribute to a shift to aerobic glycolysis that typifies metastatic progression (Ishikawa et al., 2008; Ralph et al., 2010). Relevant studies are limited by the difficulty of experimentally manipulating mtDNA of tumor cells and the paucity of tumor models with mtDNA mutations. A model of severe mtDNA damage involves mitochondrial genome deletion (King and Attardi, 1988). These ρ^0 cells grow in culture with uridine and pyruvate supplementation, but the question whether they can form tumors following autologous transplantation has not been investigated.

We have developed two stable murine tumor cell models lacking mtDNA and investigated the ability of these cells to form tumors in syngeneic mice. Our results show delayed tumor growth and acquisition of mtDNA from host cells. Cells derived from primary tumors that grow from ρ^0 cells and from their circulating and metastatic counterparts progressively recovered mitochondrial respiratory function, and this was associated with assembly of mitochondrial SCs and correlated with tumorigenicity.

RESULTS

Tumor Cells Devoid of mtDNA Show Delayed Tumor Growth

To simulate severe mitochondrial genome damage, we deleted mtDNA in metastatic murine B16 melanoma and 4T1 breast carcinoma cells using low-dose EtBr, thereby generating B16ρ^0 and 4T1ρ^0 cells that have been maintained as stable auxotrophic cell lines in the absence of EtBr for more than two years. When injected subcutaneously (s.c.) into groups of 5 syngeneic C57BL/6 (n=3) or NOD/scid (n=1) mice, B16ρ^0 cells (10^5) initiated tumors with a delay of more than 20 days compared to parental cells (Figure

1A). Intravenous (i.v.) injection of B16ρ^0 cells into NOD/scid mice failed to generate lung tumors, whereas cell lines derived from s.c. tumors and from lung metastases that grew from B16ρ^0 cells following long-term culture formed lung tumors at a similar frequency to B16 cells (Figure 1A). These cell lines were shown to be of B16 rather than host origin because they produced melanin under stress. Similarly, 4T1ρ^0 cells that are 6-thioguanine (6TG)-resistant formed tumors with a lag of 20-25 days when 10^5 cells were injected s.c. (n=6) or orthotopically into the mammary fat pad (n=1) of Balb/c mice, but failed to form lung tumors following i.v. injection (Figure 1B) or following s.c. injection of $\leq 10^4$ cells (Figure S1).

Using 6TG selection, cell lines were derived from primary tumors that formed from 4T1ρ^0 cells (4T1ρ^0SC), from circulating tumor cells (4T1ρ^0CTC) and lung metastases (4T1ρ^0SCL). When injected i.v, both 4T1ρ^0SC and 4T1ρ^0SCL cells, and a cell line derived from lung metastases that formed from an orthotopic tumor (4T1ρ^oMFPL cells), formed lung tumors that were comparable to 4T1 cells (Figure 1B). When injected s.c. into Balb/c mice, 4T1ρ^0SC cells formed tumors with a delay of ~10 days, whereas 4T1ρ^0SCL cells initiated tumors without a lag (Figure 1C, n=2). 4T1ρ^0CTC formed tumors with a lag between that of 4T1ρ^0SC and 4T1ρ^0SCL cells.

To investigate whether acquisition of tumorigenic properties was associated with respiratory competence, tissue from tumors that formed from each cell line were assessed by high-resolution respirometry. Relative to cells from parental tumors, respiration by tumors that grew from 4T1ρ^0 cells was reduced by 60% whereas 4T1ρ^0SC, 4T1ρ^0CTC and 4T1ρ^0SCL cell-derived tumors exhibited progressive recovery of respiration (Figure

1D). Histological examination of tumors derived from each cell line showed qualitative similarities (Figure 1E).

Tumors Derived from ρ^0 Cells Contain Host mtDNA and Exhibit Functional Mitochondrial Protein Synthesis

PCR analysis of the mtDNA-encoded *Cytb* gene revealed no product in B16ρ^0 or 4T1ρ^0 cells (Figure 2A). Because ρ^0 cells contain nuclear mitochondrial DNA sequences (NUMTs) and mitochondrial pseudogenes, these results exclude a significant contribution from these sources. Unexpectedly, *Cytb* was present in B16ρ^0SC and B16ρ^0SCL cells. Similar results were obtained with 4T1ρ^0SC and 4T1ρ^0SCL cells (Figure 2A). To establish the host origin of this mtDNA and to exclude the presence of latent mtDNA in ρ^0 cells, we sequenced the polymorphic mitochondrial *tRNA^{Arg}* locus. Cells from both B16ρ^0- and 4T1ρ^0-derived tumors showed the polymorphism of the host mouse (Bayona-Bafaluy et al., 2003) (Figure 2B), establishing transfer of mtDNA from host cells in the tumor microenvironment (8 consecutive adenines for C57BL/6 and 9 for NOD/SCID and Balb/c mice) to ρ^0 tumor cells in each model. To further confirm the host origin of mtDNA, we sequenced whole mtDNA from B16, B16ρ^0SC, 4T1 and 4T1ρ^0SC cells (Table S1), and identified one additional polymorphism in *Nd4* (site 10335) of B16 and B16ρ^0SC cells, and two additional polymorphisms in *16SrRNA* (site 1576) and *D-Loop* (site 16076) of 4T1 and 4T1ρ^0SC cells, confirming the host origin of mtDNA in tumors derived from B16ρ^0 and 4T1ρ^0 cells. Mitochondrial protein synthesis was shown to be functional in cell lines derived from tumors from B16ρ^0 and 4T1ρ^0 cells by the presence of COI, a mtDNA-encoded protein (Figure 2C).

Distinct Phenotypic Properties and Mitochondrial Morphology of 4T1ρ^0 Cells Following mtDNA Acquisition

Acquisition of host mtDNA by ρ^0 tumor cells prompted us to investigate the phenotypic and morphological properties of 4T1ρ^0-derived sublines, i.e. 4T1ρ^{0}SC, 4T1ρ^{0}CTC and 4T1ρ^{0}SCL cells. We also investigated 'matching' cells derived from s.c. tumors (4T1SC cells) and lung metastases (4T1SCL cells) that grew from the parental 4T1 cells. The doubling times of these cell lines were: 4T1, 18.7 h; 4T1SC, 17.5 h; 4T1SCL, 16 h; 4T1ρ^0, 33.6 h; 4T1ρ^{0}SC, 21.5 h; 4T1ρ^{0}CTC, 23.1 h; and 4T1ρ^{0}SCL, 16.1 h. Light microscopy revealed morphological differences of individual sublines (Figure 3A). Staining with EtBr confirmed the absence of mtDNA in 4T1ρ^0 cells, although nucleolar staining was evident. Co-staining with MitoTracker Red showed high mtDNA heterogeneity in 4T1ρ^{0}SC and to a lesser extent, in 4T1ρ^{0}CTC cells. Flow cytometric analysis revealed that ~60% of 4T1ρ^{0}SC cells contained little or no mtDNA, while almost 90% of 4T1ρ^{0}CTC and 100% of 4T1ρ^{0}SCL cells contained mitochondria with DNA (Figure 3B). 4T1SC cells showed similar mtDNA staining to that found in 4T1 and 4T1SCL cells (Figure S2A).

We tested individual sublines for their autophagic status, reasoning that 4T1ρ^{0}SC cells may exhibit higher mitophagy to remove respiration-defective mitochondria devoid of mtDNA. Initial acridine orange (AO) staining showed heterogeneous acidic vesicles in 4T1ρ^{0}SC cells, while western blotting (WB) revealed lower levels of the autophagy marker LC3B-II in 4T1ρ^0 and 4T1ρ^{0}SC cells than in 4T1ρ^{0}CTC and 4T1ρ^{0}SCL cells, and higher levels of p62 in 4T1ρ^{0}SC cells, both with control cells and cells treated with

the autophagy inhibitor, bafilomycin A1 (Figure 3C). The mitophagy marker, Parkin, showed increased expression in cells derived from 4T1ρ^0 and highest expression in 4T1ρ^0SCL cells, but BNIP3 expression remained unaltered in the sublines. Since individual sublines are derived from different stages of metastatic tumor progression, we investigated the markers of epithelial-mesenchymal transition (EMT), E-cadherin and vimentin. Figure 3D shows that the sublines differed coordinately in the level of expression of these markers, consistent with their different origin.

Investigation of mitochondrial morphology by transmission electron microscopy (TEM) with statistical analysis of cristae revealed that mitochondria of 4T1ρ^0 cells were distended with low-density internal staining, and were largely free of stacked cristae but contained ring-like cristae (Figure 4). Intriguingly, 4T1ρ^0SC cells showed mitochondria with and without cristae while 4T1ρ^0CTC cells contained more mitochondria with cristae. 4T1ρ^0SCL cells were indistinguishable from parental 4T1 cells and the 'matching' 4T1SC tumor cells (Figures 4, S2B).

Bioenergetics and Mitochondrial Function Following mtDNA Acquisition

Cells devoid of mtDNA use glycolysis as a source of ATP. Compared with parental 4T1 cells, 4T1ρ^0, 4T1ρ^0SC and 4T1ρ^0CTC cells showed elevated glucose uptake and increased production of lactate, and lower levels of ATP (Figure 5A-C), In contrast, 4T1ρ^0SCL cells were less glycolytic and more similar to parental 4T1 cells, as were the 'matching' sublines (Figure S3A-C). Cellular bioenergetic status and the efficiency of mitochondrial respiration modulate production of reactive oxygen species (ROS). We used the mitochondrially targeted probe, MitoSOX, to evaluate mitochondrial superoxide

generation. Cell lines from primary tumors that developed from 4T1ρ^0 cells when injected s.c. or into the mammary fat pad showed distinct intermediate and high fluorescence intensity peaks, while cells from lung metastases showed predominantly a high fluorescence intensity peak comparable with parental 4T1 cells (Figure S4A). With 4T1ρ^0 cells, only the intermediate peak was present. Similar results were obtained with B16 cells (Figure S4B). Quantitation of MitoSOX staining showed low fluorescence in 4T1ρ^0 cells with other sublines being comparable with parental 4T1 cells (Figure 5D). Dihydrodichlorofluorescein (DCF) measurement of cytosolic hydrogen peroxide showed non-significant reduction in the signal in 4T1ρ^0, 4T1ρ^0SC and 4T1ρ^0SCL cells relative to parental 4T1 cells (Figure 5E). Using TMRM as a probe, mitochondrial membrane potential ($\Delta\Psi_m$) was found to be similar in 4T1and 4T1ρ^0 cells, elevated in 4T1ρ^0SCL and to a lesser extent in 4T1ρ^0SC cells, and was greatly reduced in 4T1ρ^0CTC cells (Figure 5F).

Respiration Recovery Following mtDNA Acquisition by 4T1ρ^0 Cells

4T1ρ^0 cells showed barely detectable respiration, which was low in 4T1ρ^0SC cells and higher in 4T1ρ^0CTC cells, while 4T1ρ^0SCL cells respired at a rate similar to that of parental cells (Figures 5G and S5A). Respiration was similar in 4T1 and 4T1SC cells and slightly lower in 4T1SCL cells (Figure S3F). Respiration *via* CI and CII was very low in 4T1ρ^0SC cells and higher in 4T1ρ^0CTC cells. Respiration *via* CI was similar in parental cells and 4T1ρ^0SCL while respiration *via* CII was highly elevated in metastatic cells (Figures 5H and S5B). A similar respiration profile was found for isolated mitochondria (Figure S5C), indicating that respiration of the sublines is primarily governed by

mitochondria and not the extra-mitochondrial compartment. Collectively, these results show significant differences in respiration of individual 4T1ρ^0-derived sublines, which paralleled the efficacy of these cells to initiate tumor growth (Figure 1C).

mtDNA Recovery and Transcription Following mtDNA Acquisition

To determine whether phenotypic differences in 4T1ρ^0-derived sublines following mtDNA acquisition were related to gradual restoration of mtDNA, we evaluated the mtDNA/nDNA ratio. While 4T1ρ^0 cells did not contain mtDNA, we found a several-fold increase in the mtDNA/nDNA ratio in 4T1ρ^0SC cells compared with parental cells. This high ratio was maintained over several months of the cells in culture (Figure 6A). 4T1ρ^0CTC and 4T1ρ^0SCL cells showed ratios more similar to those of parental cells as did the 'matching' 4T1SC and 4T1SCL cells (Figure S3G). No transcripts of mtDNA-encoded genes were found in 4T1ρ^0 cells, but these were transcribed in 4T1ρ^0-derived sublines. Relative to 4T1 cells *Nd1, Nd2, Nd4, Nd4l, Nd5, Nd6* and *mt-Co2* were elevated 2-4-fold in 4T1ρ^0SC cells, and *Nd1, Nd2, mt-Co2, Atp6* and *Atp8* elevated 1.5-4.5-fold in 4T1ρ^0SCL cells. The level of the *D-loop* transcript was similar in all 4T1ρ^0-derived sublines, indicating that the regulatory region of mtDNA does not hinder mtDNA replication or transcription in these cells (Figure 6B).

Nuclear DNA-encoded subunits of mitochondrial complexes, with the exception of S*dhc*, showed a similar expression pattern across the cell lines, indicating a common mechanism regulating their transcription (Figure 6C). Of the regulatory genes, the relative level of mRNA for the mitochondrial transcription factor, *Tfam*, was very low in 4T1ρ^0, and almost 3-fold higher in 4T1ρ^0SC cells, but similar to 4T1 cells in 4T1ρ^0CTC

and 4T1ρ^{0}SCL cells (Figure 6D). The *Tfam* transcript profile in the sub-lines mirrors the mtDNA/nDNA ratios, suggesting a causal relationship. *Nrf1*, *Nrf2*, *Tfb1m*, *Tfb2m* and *Top1m* transcripts were depressed in 4T1ρ^{0}SC cells, while the assembly factor *Scafi (Cox7a2l)* was decreased in 4T1ρ^0, 4T1ρ^{0}SC and 4T1ρ^{0}CTC cells, and the assembly factor *Hig2a* was relatively unchanged. No differences in these transcripts were observed in the 'matching' cells (Figure S3H).

Mitochondrial Protein Synthesis, and Citrate Synthase (CS) and CII Activity Following mtDNA Acquisition

We next studied translation of mtDNA-encoded proteins. Figure 7A shows only background staining in 4T1ρ^0 cells, with the proteins coordinately translated 2-3-times more efficiently in the other sublines compared with parental cells. Activity of CS, the first enzyme of the TCA cycle, was increased 2.5-fold in 4T1ρ^0 and 4T1ρ^{0}SC cells, while in 4T1ρ^{0}CTC and 4T1ρ^{0}SCL cells the activity was similar to that in parental cells (Figure 7B). This increase was not observed in the 'matching' sublines (Figure S3I). We did not see a major difference in succinate dehydrogenase (SDH) activity in sublines derived from 4T1ρ^0 cells (Figure 7C) or the 'matching' cells (Figure S3J). Succinate quinone reductase (SQR) activity of CII was very low in 4T1ρ^0, 4T1ρ^{0}SC and 4T1ρ^{0}CTC cells, while in 4T1ρ^{0}SCL cells it was 70% higher than in 4T1 cells (Figure 7D). SQR activity was about 2-fold higher in the metastatic 4T1SCL cells than in 4T1 and 4T1SC (Figure S3K).

Respiratory Complex Assembly and Subunit Expression Following mtDNA Acquisition

To determine the steady-state level of proteins representing subunits of RCs encoded by mtDNA and nDNA, as well as proteins with a regulatory or more general role in mitochondria, we performed WB following SDS-PAGE on 4T1ρ^0-derived and parental cells (Figure 7E and S3L). The nDNA-encoded CI subunits NDUFS3 and NDUFA9 were not expressed in 4T1ρ^0 cells but were expressed in all other cell lines. The CII subunit SDHA was highly expressed in all cell lines while SDHB was less highly expressed in 4T1ρ^0, 4T1ρ^0SC and 4T1ρ^0SCL cells. The assembly factor SDHAF2 that flavinates SDHA was expressed in all cell lines but more strongly in 4T1ρ^oSC cells, while the nuclear-encoded CIII protein, Core2, was expressed in all sulines but was lower in 4T1ρ^0 cells. The nuclear-encoded CV protein, ATPaseβ, was expressed similarly in all sublines. The mtDNA-encoded COI and nDNA-encoded COIV subunits of CIV were not expressed in 4T1ρ^0 cells with COI being highest in 4T1ρ^0SC cells. nDNA-encoded proteins that are not part of RCs were expressed in all sub-lines with Cyt c being particularly high in 4T1ρ^0 cells, and TIM23 and VDAC1 attenuated in these cells. PGCα/β that regulates the transcription factors NRF1/NRF2 was poorly expressed in 4T1ρ^0 cells. OPA1, which modulates cristae formation and geometry, was low in 4T1ρ^0 and 4T1ρ^0SC cells, and progressively increased in 4T1ρ^0CTC and 4T1ρ^0SCL cells, while it was high in 'matching' 4T1SC and 4T1SCL cells (Figure S3L).

Native blue gel electrophoresis (NBGE) using a mild detergent followed by WB was employed to assess the assembly of individual RCs and SCs (Figure 7F). Parental cells showed a high level of the fully assembled respirasome (CI+$CIII_2$+CIV_n), which

was absent in 4T1ρ^0 cells. Low respirasome levels were observed in 4T1ρ^0SC cells and 4T1ρ^0CTC cells, and full restoration was observed in 4T1ρ^0SCL cells. Free CI, CIII in the form of a dimer and in an SC with CIV, and CIV largely in the form of a monomer, were present at similar levels in all cell types except for 4T1ρ^0 cells. CV was partially assembled in 4T1ρ^0 cells due to the absence of structural mtDNA-encoded ATP6 and ATP8, while it was fully assembled and present as a dimer in all other cell types. CII was represented in 4T1ρ^0 cells by the highly expressed SDHA subunit. SDHB, only observed in fully assembled CII, was lower in 4T1ρ^0, 4T1ρ^0SC and 4T1ρ^0CTC than in 4T1 cells and elevated by 70% in 4T1ρ^0SCL cells. These findings document that transition from 4T1ρ^0CTC to 4T1ρ^0SCL cells yields a fully assembled respirasome and CII, associated with efficient respiration and tumor initiation.

DISCUSSION

Whole genome approaches have deepened to our understanding of the role of mutations in nDNA in different cancers (Kandoth et al., 2013; Khurana et al., 2013). Mutations in mtDNA have also been described in cancer, but their contribution to tumor initiation, progression and metastasis is less clear (Brandon et al., 2006; Wallace, 2012; Schon et al., 2012). Functionally relevant mtDNA mutations may be expected to compromise mitochondrial respiration and promote aerobic glycolysis, a bioenergetic trait of many tumors. In breast cancer, mtDNA mutations and low mtDNA copy number are associated with increased metastasis and poor prognosis (Petros et al., 2005, Tseng et al., 2006), while a recent study showed that low mtDNA copy number promotes metastasis by inducing EMT via mitochondrial retrograde signaling (Guha and Avadhani, 2013).

Using highly metastatic murine tumor models with mtDNA deletion to simulate severe mtDNA damage, we have found a long lag to tumor formation for both B16ρ^0 melanoma and 4T1ρ^0 breast carcinoma cells in C57BL/6 and Balb/c mice respectively, as well as in the NOD/scid animals. Previous reports on grafting human ρ^0 tumor cells have provided variable results, depending on the tumor type, the site of injection and the recipient (Hayashi et al., 1992; Morais et al., 1994; Cavelli et al., 1997; Magda et al., 2008; Kulaweic et al., 2008; Imanishi et al., 2011). In both our models, delayed tumor growth was observed, and was associated with mtDNA acquisition from the host suggestive of horizontal mtDNA transfer. This was demonstrated when cells derived from tumors that grew from B16ρ^0 and 4T1ρ^0 cells were found to be positive for both the *Cytb* gene and COI protein. We excluded the possibility of latent mtDNA being present in ρ^0 cells by showing that tumors growing from B16ρ^0 and 4T1ρ^0 cells contained the *tRNA*^{Arg} gene polymorphism of the host mouse (Bayona-Bafaluy et al., 2006) which is distinct from that of the original tumor. This notion is corroborated by our identification of additional polymorphisms in B16ρ^0SC and 4T1ρ^0SC cells that are identical with the host and distinct from parental cells, which, when taken together with the *tRNA*^{Arg} polymorphism unequivocally prove the host origin of the mtDNA.

Because there is no known mechanism for intercellular transfer of mtDNA across both mitochondrial inner and outer membranes and the plasma membrane, transfer of whole mitochondria is the most likely explanation. This has previously been shown to occur *in vitro* (Spees et al., 2006; Cho et al., 2012; Gerdes and Carvalho, 2008; Gurke et al., 2008) and in a mouse model of acute lung injury, documenting mitochondrial transfer from mesenchymal stem cells (MSCs) injected into the animal's lungs (Islam et al., 2012). Organelle transfer between cells has been reviewed recently, with a number of

reports documenting mitochondrial transfer (Rogers and Bhattacharya, 2013). Phylogenetic evidence also supports mtDNA transfer between cells as shown in a transmissible canine venereal tumor (Rebbeck et al., 2011).

To better understand the role of mitochondrial respiration in tumorigenesis and metastasis, we characterized malignant cells from different tumor microenvironments in the 4T1ρ^0 tumor model. To ensure that the results relate to mtDNA acquisition and not local microenvironment effects, we isolated 'matching' cell lines from primary s.c. 4T1 tumors and from lung metastases. Of interest was the finding that cells derived from primary tumors that grew from 4T1ρ^0 cells still exhibited a considerable delay in tumor initiation, while the kinetics of growth of tumors derived from the metastatic 4T1ρ^0SCL cells showed no delay in tumor initiation. These findings, initially acquired in our laboratory in Wellington, New Zealand, were repeated with almost identical results in our other laboratory in Prague, Czech Republic, 9 months later, indicating the robust nature of the results and their high reproducibility.

The most striking finding is the stepwise recovery of mitochondrial respiration from undetectable levels in ρ^0 cells to low levels in primary tumor cells derived from ρ^0 cells, progressing to higher levels of respiration in CTCs and full restoration in metastatic cells. The phenotype of the individual cell types was maintained in culture, as documented by sustained high mtDNA/nDNA ratio in cells from the primary tumor. This suggests that these cells are unable to restore full mitochondrial function during long-term maintenance *in vitro* and need microenvironmental exposure to progress to full respiratory competence. Our findings are consistent with earlier *in vitro* results (Spees et al., 2006) showing that mitochondrial transfer from MSCs and skin fibroblasts to human A549ρ^0 lung adenocarcinoma cells restored their respiratory capacity.

We provide detailed analysis of the individual stages of recovery of respiratory competence from parental cells to their metastatic counterparts, documenting each 'recovery' stage. We show that a crucial step of full respiration recovery is associated with the assembly of the respirasome and CII, with SDH activity being a component of the TCA cycle as well as OXPHOS that is compromised in ρ^0 cells. This is also supported by the high level of SQR activity in metastatic cells. Our results show that the level of the assembly factor SCAFI (Lapuente-Brun et al., 2013), but not HIG2A (Moreno-Lastres et al., 2012), correlates with the extent of respirasome assembly in tumors derived from 4T1ρ^0 cells. The key regulatory role of SCAFI and other respirasome assembly factors in the tumor microenvironment in metastatic progression needs further investigation. Similarly, the reasons for full assembly of CII in metastatic cells are not known but are likely to be linked to retrograde mitochondrial signaling. That assembly of the RCs and SCs is crucial for the full recovery of mitochondrial respiration is evidenced by our findings that except for ρ^0 cells, sublines of these cells exhibited transcriptional and translational activity of mtDNA-encoded genes, with fully-assembled CI, CIII and CIV being present. A key to understanding the different behaviors of the sublines may relate to the high level of mitochondrial heterogeneity.

Our findings raise several challenging questions. A fundamental one relates to how ρ^0 cells, having acquired mtDNA, progress from primary tumor via the circulation to lung metastases, and how this progression leads to full recovery of respiration. In our model, metastatic potential is encoded in the nuclear genome but suppressed by the absence of mtDNA. Acquisition of 'normal' mtDNA from the microenvironment enables 4T1ρ^0 cells to grow as primary tumors and to 'unleash' their metastatic potential. It is possible that rare cells acquire one or a few mitochondria that contain mtDNA and that

these cells replicate their mtDNA, build cisternal structures of cristae and multiply clonally at the expense of cells lacking mtDNA that are progressively eliminated by autophagy. Our finding that autophagic activity is low in 4T1ρ^0 and 4T1ρ^0SC cells that also have very low respiration is consistent with a report showing faulty autophagy in cells with suppressed ETC (Graef and Nunnari, 2011). Such cells do not appear to 'clear' malfunctional mitochondria, which is more likely to occur at the stage of CTCs, where respiration is partially restored and autophagy is higher.

Quantification of mtDNA/nDNA ratios showed stable elevation in 4T1ρ^0SC cells, consistent with high levels of TFAM, a factor critical for replication, transcription and packaging of mtDNA (Kukat and Larsson, 2013). Compromised respiration is correlated with lack of cristae in all 4T1ρ^0 cells and poorly formed cristae in many 4T1ρ^0SC cells, consistent with low OPA1 levels (Cogliati et al., 2013). The reasons why ρ^0 cells that have acquired mtDNA require conditioning by their local microenvironment to restore a parental intracellular distribution of mtDNA are not clear, but may relate to progressive changes in mitochondria-to-nucleus retrograde signaling that eventually normalizes both mtDNA distribution and respiratory function. The importance of the tumor microenvironment is corroborated by the finding that 4T1 cells show both epithelial and mesenchymal markers, highly localized within the cell and exhibiting different patterns of compartmentalization, with coordinate changes in E-cadherin and vimentin staining across 4T1 cells and derived sublines confirming the different origins of the individual 4T1 sublines.

The signals that ρ^0 cells employ to acquire mtDNA from stromal cells as well as how this process occurs are unclear. It has been proposed that cells form tunneling nanotubes to move biomaterial between cells (Rustom et al., 2004; Gerdes and Carvalho,

2008), as shown for the mobilization of organelles (Rustom et al., 2004; Koyanagi et al., 2005; Lou et al., 2012; Islam et al., 2012; Pasquier et al., 2013); this process is suppressed by cytochalasin B (Bukoreshtliev et al., 2009). Other mechanisms of organelle trafficking between cells have also been proposed including membrane vesicles, cell fusion and various other cytoplasmic bridging processes. Of importance is the minimum level of mtDNA damage needed to initiate intercellular transfer of functional mitochondria. It has been shown that a gradual decrease in the number of mtDNA copies in human glioblastoma cells eventually results in a phenotype unable to recover *in vitro*, while injecting these cells into immunocompromized mice resulted in delayed formation of tumors and restoration of mitochondrial function (Dickinson et al., 2013). Another important question is how recovering mitochondria signal to the nucleus to trigger transcription of genes needed for mitochondrial function. Retrograde mitochondrial signaling is poorly understood at present and may include the bioenergetic status of the cell (e.g. the AMP/ATP ratio), the level of ROS, release of metabolites, Ca^{2+}, etc (Liu and Butow, 2006; Moreno-Loshuertos et al., 2006; Ryan and Hoogenraad, 2007, Guha and Avadhani, 2013).

In conclusion, we have shown that tumor cells devoid of mtDNA, a model of extensive mtDNA damage, can acquire mtDNA of host origin, resulting in stepwise recovery of respiration from primary to metastatic tumor cells. We show that a crucial aspect of full recovery of mitochondrial respiration is full assembly of the respirasome and CII, which are directly linked with efficient tumor formation. To our knowledge, this is the first report of *in vivo* mitochondrial genome acquisition by tumor cells with compromised respiration due to mtDNA deletion, and demonstrates that mitochondrial respiration is required for tumorigenesis in these autologous models. Mitochondrial DNA

mutations can also contribute to tumorigenesis, suggesting that optimum bioenergetic balance may relate to the individual tumor (Tan et al., 2013). Our results support the notion of tumor plasticity and involving exceptional ability to overcome unfavorable situations (Hanahan and Weinberg, 2011).

EXPERIMENTAL PROCEDURES

Cell Culture, Tumor Formation and Establishment of Tumor-Derived Cells. B16 and 6TG-resistant 4T1 cells (Tan and Berridge, 2004) from ATCC were used. Cell maintenance, preparation of ρ^0 cells and the establishment of tumors and tumor-derived cell cultures are described in detail in the Supplementary Text.

Mitochondria Isolation and Sequence Analysis

Functional mitochondrial were isolated according to Schmitt et al (2013) and mtDNA *tRNA*^{Arg} sequencing carried out on a PCR-amplified region using Sanger sequencing. Whole mtDNA sequencing used overlapping PCR amplified products and both Ion Torrent and Nanopore MinION approaches.

Microscopic and Flow Cytometric Cell Evaluation. Standard methodology described in more detail in the Supplementary Text was used for bright field and fluorescence microscopy and TEM, while flow cytometry used a BD FACScalibur.

Respiration Assays. Cellular respiration was evaluated using an Oxygraph-2k instrument (Oroboros Instruments) and published procedures (Pesta and Gnaiger, 2012), as detailed in the Supplementary Text.

Mitochondrial Biochemistry Assays and Gene Expression Analysis

Mitochondrial membrane potential and ROS production were measured by flow cytometry using the fluorescent probes TMRM, DCF-DA and MitoSOX. Glucose uptake

was measured using 2-NGDG, ATP using a luciferase-based assay and lactate colorimetrically. *Cytb* was measured by PCR product, while gene expression analysis used qRT-PCR. Western blotting and NBGE used well-established methods while newly-synthesisized mitochondrial proteins were evaluated using a Clik-iT AHA kit followed by Western blotting.

Statistical Analysis. Unless stated otherwise, data are mean ± S.D of at least three independent experiments or used groups of 5 mice. The two-tailed unpaired Student's t test was used to assess statistical significance with $p<0.05$ being regarded as significant. Images are representative of three independent experiments. For TEM data, Tukey's multiple comparison procedure and statistical test was used at $p<0.05$.

ACKNOWLEDGEMENTS

We thank H. Matilainen for help with the orthotopic tumor model, J. Janacek for help with statistical analysis of the TEM data, and I. Wittig for critical reading of the manuscript. This research was supported in part by Genesis Oncology Trust, the Cancer Society of New Zealand, the Breast Cancer Research Trust and by the Malaghan Institute to M.V.B., grants from the National Health and Medical Research Council, Cancer Council Queensland, Clem Jones Foundation and the Czech Science Foundation P301/10/1937 to J.N., grant from the Australian Research Council to J.N and L.D.F., and grants from the Czech Science Foundation P305/12/1708 to J.T and P301/12/1851 to J.R. L.D.F. was supported in part by a Griffith University Senior Research Fellowship. This project was supported in part by the BIOCEV European Regional Development Fund CZ.1.05/1.1.00/02.0109.

REFERENCES

Acin-Perez, R., Fernandez-Silva, R., Peleato, M.L., Perez-Martos, A., and Enriquez, J.A. (2008). Respiratory active mitochondrial supercomplexes. Mol. Cell *32*, 529-539.

Althoff, T., Mills, D.J., Popot, J.L., and Kühlbrandt, W. (2011). Arrangement of electron transport chain components in bovine mitochondrial supercomplex I1III2IV1. EMBO J. *30*, 4652-4664.

Barrientos, A., Fontanesi, F., and Diaz, F. (2009). Evaluation of the mitochondrial respiratory chain and oxidative phosphorylation system using polarography and spectrophotometric enzyme assays. Curr. Protoc. Hum. Genet. Chapter 19**,** unit19.3.

Bayona-Bafaluy, M.P., Acín-Pérez, R., Mullikin, J.C., Park, J.S., Moreno-Loshuertos, R., Hu, P., Pérez-Martos, A., Fernández-Silva, P., Bai, Y., and Enríquez, J.A. (2003). Revisiting the mouse mitochondrial DNA sequence. Nucleic Acids Res. *31*, 5349-5355.

Brandon, M., Baldi, P., and Wallace, D.C. (2006). Mitochondrial mutations in cancer. Oncogene *25*, 4647-4662.

Bukoreshtliev, N.V., Wang, X., Hodneland, E., Gurke, S., Barroso, J.F., and Gerdes, H.H. (2009). Selective block of tunneling nanotube (TNT) formation inhibits intercellular organelle transfer between PC12 cells. FEBS Lett. *583*, 1481-1488.

Cavalli, L.R., Varella-Garcia, M., and Liang, B.C. (1997). Diminished tumorigenic phenotype after depletion of mitochondrial DNA. Cell Growth Differ. *8*, 1189-1198.

Cho, Y.M., Kim, J.H., Kim, M., Park, S.J., Koh, S.H., Ahn, H.S., Kang, G.H., Lee, J.B., Park, K.S., and Lee, H.K. (2012). Mesenchymal stem cells transfer mitochondria to the cells with virtually no mitochondrial function but not with pathogenic mtDNA mutations. PLoS One *7*, e32778.

Cogliati, S., Frezza, C., Soriano, M.E., Varanita, T., Quintana-Cabrera, R., Corrado, M., Cipolat, S., Costa, V., Casarin, A., Gomes, L.C., et al. (2013). Mitochondrial cristae shape determines respiratory chain supercomplexes assembly and respiratory efficiency. Cell *155*, 160-171.

DeBerardinis, R.J., Mancuso, A., Daikhin, E., Nissim, I., Yudkoff, M., Wehrli, S., and Thompson, C.B. (2007). Beyond aerobic glycolysis: transformed cells can engage in glutamine metabolism that exceeds the requirement for protein and nucleotide synthesis. Proc. Natl. Acad. Sci. USA *104*, 19345-19350.

De Carvalho, D.D., You, J.S., and Jones, P.A. (2010). DNA methylation and cellular reprogramming. Trends Cell Biol. *20*, 609-617.

Dickinson, A., Yeung, K.Y., Donoghue, J., Baker, M.J., Kelly, R.D., McKenzie, M., Johns, T.G., and St John, J.C. (2013). The regulation of mitochondrial DNA copy number in glioblastoma cells. Cell Death Differ. 20, 1644-1653.

Dong, L.F., Low, P., Dyason, J.C., Wang, X.F., Prochazka, L., Witting, P.K., Freeman, R., Swettenham, E., Valis, K., Liu, J., et al (2008). α-Tocopheryl succinate induces apoptosis by targeting ubiquinone-binding sites in mitochondrial respiratory complex II. Oncogene *27*, 4324-4335.

Falkenberg, M., Larsson, N.G., and Gustafsson, C.M. (2007). DNA replication and transcription in mammalian mitochondria. Annu. Rev. Biochem. *76*, 679-699.

Gerdes, H.H., and Carvalho, R.N. (2008). Intercellular transfer mediated by tunneling nanotubes. Curr. Opin. Cell Biol. *20*, 470-475.

Graef, M., and Nunnari, J. (2011). Mitochondria regulate autophagy by conserved signalling pathways. EMBO J *30*, 2101-2114.

Guha, M., and Avadhani, N.G. (2013) Mitochondrial retrograde signaling at the crossroads of tumor bioenergetics, genetics and epigenetics. Mitochondrion *13*, 577-591.

Guha, M., Srinivasan, S., Ruthel, G., Kashina, A.K., Carstens, R.P., Mendoza, A., Khanna, C., Van Winkle, T., and Avadhani, N.G. Mitochondrial retrograde signaling induces epithelial-mesenchymal transition and generates breast cancer stem cells. Oncogene, doi: 10.1038/onc.2013.467.

Gurke, S., Barroso, J.F., Hodneland, E., Bukoreshtliev, N.V., Schlicker, O., and Gerdes, H.H. (2008). Tunneling nanotube (TNT)-like structures facilitate a constitutive, actomyosin-dependent exchange of endocytic organelles between normal rat kidney cells. Exp. Cell Res. *314*, 3669-3683.

Hanahan, D., and Weinberg, R.A. (2011). Hallmarks of cancer: the next generation. Cell *144*, 646-674.

Hayashi, J., Takemitsu, M., and Nonaka, I. (1992). Recovery of the missing tumorigenicity in mitochondrial DNA-less HeLa cells by introduction of mitochondrial DNA from normal human cells. Somat. Cell Mol. Genet. *18*, 123-129.

Herst, P.M., and Berridge, M.V. (2007). Cell surface oxygen consumption: a major contributor to cellular oxygen consumption in glycolytic cancer cell lines. Biochim. Biophys. Acta *1767*, 170-177.

Herst, P.M., Howman, R.A., Neeson, P.J., Berridge, M.V., and Ritchie, D.S. (2011). The level of glycolytic metabolism in acute myeloid leukemia blasts at diagnosis is prognostic for clinical outcome. J. Leukocyte Biol. *89*, 51-55.

Ikeda, K., Shiba, S., Horie-Inoue, K., Shimokata, K., and Inoue, S. (2013). A stabilizing factor for mitochondrial respiratory supercomplex assembly regulates energy metabolism in muscle. Nat. Commun. *4*, 2147.

Imanishi, H., Hattori, K., Wada, R., Ishikawa, K., Fukuda, S., Takenaga, K., Nakada, K., and Hayashi, J. (2011) Mitochondrial DNA mutations regulate metastasis of human breast cancer cells. PLoS One *6*, e23401.

Ishikawa, K., Takenaga, K., Akimoto, M., Koshikawa, N., Yamaguchi, A., Imanishi, H., Nakada, K., Honma, Y., and Hayashi, J. (2008). ROS-generating mitochondrial DNA mutations can regulate tumor cell metastasis. Science *320*, 661-664.

Islam, M.N., Das, S.R., Emin, M.T., Wei, M., Sun, L., Westphalen, K., Rowlands, D.J., Quadri, S.K., Bhattacharya, S., and Bhattacharya, J. (2012). Mitochondrial transfer from bone-marrow-derived stromal cells to pulmonary alveoli protects against acute lung injury. Nat. Med. *18*, 759-765.

Kandoth, C., McLellan, M.D., Vandin, F., Ye, K., Niu, B., Lu, C., Xie, M., Zhang, Q., McMichael, J.F., Wyczalkowski, M.A., et al. (2013). Mutational landscape and significance across 12 major cancer types. Nature *502*, 333-339.

King, M.P., and Attardi, G. (1988). Injection of mitochondria into human cells leads to a rapid replacement of the endogenous mitochondrial DNA. Cell *52*, 811-819.

King, M.P., and Attardi, G. (1989). Human cells lacking mtDNA: repopulation with exogenous mitochondria by complementation. Science *246*, 500-503.

Khurana, E., Fu, Y., Colonna, V., Mu, X.J., Kang, H.M., Lappalainen, T., Sboner, A., Lochovsky, L., Chen, J., Harmanci, A., et al. (2013). Integrative annotation of variants from 1092 humans: application to cancer genomics. Science *342*, 84.

Koyanagi, M., Brandes, R.P., Haendeler, J., Zeiher, A.M., and Dimmeler, S. (2005). Cell-to-cell connection of endothelial progenitor cells with cardiac myocytes by nanotubes: a novel mechanism for cell fate changes? Circ Res. *96*, 1039-1041.

Krishnan, K.J., Reeve, A.K., Samuels, D.C., Chinnery, P.F., Blackwood, J.K., Taylor, R.W., Wanrooij, S., Spelbrink, J.N., Lightowlers, R.N., and Turnbull, D.M. (2008). What causes mitochondrial DNA deletions in human cells? Nat. Genet. *40*, 275-279.

Kroemer, G., and Pouyssegur, J. (2008). Tumor cell metabolism: cancer's Achilles' heel. Cancer Cell *13*, 472-482.

Kukat, C., and Larsson, N.G. (2013). mtDNA makes a U-turn for the mitochondrial nucleoid. Trends Cell Biol. *23*, 457-463.

Kulawiec, M., Safina, A., Desouki, M.M., Still, I., Matsui, S., Bakin, A., Singh, K.K. (2008). Tumorigenic transformation of human breast epithelial cells induced by mitochondrial DNA depletion. Cancer Biol. Ther. *7*, 1732-1743.

Lapuente-Brun, E., Moreno-Loshuertos, R., Acín-Pérez, R., Latorre-Pellicer, A., Colás, C., Balsa, E., Perales-Clemente, E., Quirós, P.M., Calvo, E., Rodríguez-Hernández, M.A., et al. (2013). Supercomplex assembly determines electron flux in the mitochondrial electron transport chain. Science *340*, 1567-1570.

Liu, Z., and Butow, R.A. (2006). Mitochondrial retrograde signaling. Annu. Rev. Genet. *40*, 159-185.

Lou, E., Fujisawa, S., Morozov, A., Barlas, A., Romin, Y., Dogan, Y., Gholami, S., Moreira, A.L., Manova-Todorova, K., and Moore, M.A. (2012). Tunneling nanotubes provide a unique conduit for intercellular transfer of cellular contents in human malignant pleural mesothelioma. PLoS One *7*, e33093.

Lu, J., Sharma, L.K., and Bai, Y. (2009). Implications of mitochondrial DNA mutations and mitochondrial dysfunction in tumorigenesis. Cell Res. *19*, 802-815.

Magda, D., Lecane, P., Prescott, J., Thiemann, P., Ma, X., Dranchak, P.K., Toleno, D.M., Ramaswamy, K., Siegmund, K.D., and Hacia, J.G. (2008) mtDNA depletion confers specific gene expression profiles in human cells grown in culture and in xenograft. BMC Genomics *9*, 521.

Morais, R., Zinkewich-Péotti, K., Parent, M., Wang, H., Babai, F., and Zollinger, M. (1994). Tumor-forming ability in athymic nude mice of human cell lines devoid of mitochondrial DNA. Cancer Res. *54*, 3889-3896.

Moreno-Lastres, D., Fontanesi, F., García-Consuegra, I., Martín, M.A., Arenas, J., Barrientos, A., and Ugalde, C. (2012). Mitochondrial complex I plays an essential role in human respirasome assembly. Cell Metab. *15*, 324-335.

Moreno-Loshuertos, R., Acín-Pérez, R., Fernández-Silva, P., Movilla, N., Pérez-Martos, A., Rodriguez de Cordoba, S., Gallardo, M.E., and Enríquez, J.A. (2006). Differences in reactive oxygen species production explain the phenotypes associated with common mouse mitochondrial DNA variants. Nat. Genet. *38*, 1261-1268.

Neupert, W., and Herrmann, J.M. (2007). Translocation of proteins into mitochondria. Annu. Rev. Biochem. *76*, 723-749.

Pasquier, J., Guerrouahen, B.S., Al Thawadi, H., Ghiabi, P., Maleki, M., Abu-Kaoud, N., Jacob, A., Mirshahi, M., Galas, L., Rafii, S., et al. (2013). Preferential transfer of mitochondria from endothelial to cancer cells through tunneling nanotubes modulates chemoresistance. J. Transl. Med. *11*, 94.

Pesta, D., and Gnaiger, E. (2012). High-resolution respirometry: OXPHOS protocols for human cells and permeabilized fibers from small biopsies of human muscle. Methods Mol. Biol. *810*, 25-58.

Petros, J.A., Baumann, A.K., Ruiz-Pesini, E., Amin, M.B., Sun, C.Q., Hall, J., Lim, S., Issa, M.M., Flanders, W.D., Hosseini, S.H., et al. (2005). mtDNA mutations increase tumorigenicity in prostate cancer. Proc. Natl. Acad. Sci. USA. *102*, 719-724.

Plass, C., Pfister, S.M., Lindroth, A.M., Bogatyrova, O., Claus, R., and Lichter, P. (2013) Mutations in regulators of the epigenome and their connections to global chromatin patterns in cancer. Nat. Rev. Genet. *14*, 765-780.

Ralph, S.J., Rodríguez-Enríquez, S., Neuzil, J., Saavedra, E., and Moreno-Sánchez, R. (2010). The causes of cancer revisited: ‘‘Mitochondrial malignancy” and ROS-induced oncogenic transformation - Why mitochondria are targets for cancer therapy. Mol. Asp. Med. *31*, 145-170.

Rebbeck, C.A., Leroi, A.M., and Burt, A. (2011). Mitochondrial capture by a transmissible cancer. Science *331*, 303.

Rogers, R.S. and Bhattacharya, J. (2013). When cells become organelle donors. Physiology *28*, 414-422.

Rustom, A., Saffrich, R., Markovic, I., Walther, P., and Gerdes, H.H. (2004). Nanotubular highways for intercellular organelle transport. Science *303*, 1007-1010.

Ryan, M.T., and Hoogenraad, N.J. (2007). Mitochondrial-nuclear communications. Annu. Rev. Biochem. *76*, 701-722.

Schägger, H., and Pfeiffer, K. (2011). Supercomplexes in the respiratory chains of yeast and mammalian mitochondria. EMBO J. *19*, 1777-1783.

Schmitt, S., Saathoff, F., Meissner, L., Schropp, E. M., Lichtmannegger, J., Schulz, S., Eberhagen, C., Borchard, S., Aichler, M., Adamski, J., Plesnila, N., Rothenfusser, S., Kroemer, G., and Zischka, H. (2013). A semi-automated method for isolating functionally intact mitochondria from cultured cells and tissue biopsies. Anal. Biochem. *443*, 66-74.

Schon, E.A., DiMauro, S., and Hirano, M. (2012). Human mitochondrial DNA: roles of inherited and somatic mutations. Nat. Rev. Genet. *13*, 878-890.

Spees, J.L., Olson, S.D., Whitney, M.J., and Prockop, D.J. (2006). Mitochondrial transfer between cells can rescue aerobic respiration. Proc. Natl. Acad. Sci. USA *103*, 1283-1288.

Surani, M.A. (2001). Reprogramming of genome function through epigenetic inheritance. Nature *414*, 122-128.

Tan, A.S., Baty, J.W. and Berridge, M.V. (2014). The role of mitochondrial electron transport in tumorigenesis and metastasis. Biochim. Biophys. Acta *1840*, 1454-1463.

Tseng, L.M., Yin, P.H., Chi, C.W., Hsu, C.Y., Wu, C.W., Lee, L.M., Wei, Y.H., and Lee, H.C. (2006). Mitochondrial DNA mutations and mitochondrial DNA depletion in breast cancer. Genes Chromosomes Cancer *45*, 629-638.

Vander Heiden, M.G., Cantley, L.C., and Thompson, C.B. (2009). Understanding the Warburg effect: the metabolic requirements of cell proliferation. Science *324*, 1029-1033.

Wallace, D.C. (2012). Mitochondria and cancer. Nat. Rev. Cancer *12*, 685-698.

Wallace, D.C., and Fan, W. (2010). Energetics, epigenetics, mitochondrial genetics. Mitochondrion *10*, 12-31.

Wittig, I, Braun, H.P., and Schägger, H. (2006). Blue native PAGE. Nat. Protoc. *1*, 418-428.

FIGURE LEGENDS

Figure 1. Tumor Cells lacking mtDNA Show Delayed Tumor Growth (A) B16 and B16ρ^0 cells (10^5) were injected s.c. into C57BL/6 or NOD/scid mice and tumor growth monitored. These cells, and cell lines derived from s.c. tumors and lung metastases that grew from B16ρ^0 cells were also injected i.v. into NOD/scid mice, and lung weight and tumor colonies determined. (B) 4T1 and 4T1ρ^0 cells were injected s.c. or orthotopically into the mammary fat pad of Balb/c mice and tumor growth monitored. These cells and 6TG-resistant cell lines derived from s.c. tumors and lung metastases that grew from 4T1ρ^0 cells were also injected i.v. into Balb/c mice and lung weight and tumor colonies determined. Images of lungs from these mice are also shown. (C) 4T1, 4T1ρ^0, 4T1ρ^0SC, 4T1ρ^0CTC and 4T1ρ^0SCL cells were injected into Balb/c mice and tumor growth monitored. (D) Oxygen consumption by tissue of tumors derived from cells as stated above (C) was compared with respiration of liver tissue obtained from the same mice. (E) Histological staining of tissue sections from (C) stained with H & E; size bar 20 μm. The data are derived from three independent experiments and the results expressed as mean values ± S.D. The symbol '*' documents significantly significant differences with $p<0.05$ and '***' $p<0.001$.

Figure 2. Tumors Derived from mtDNA-Deficient Cells Contain mtDNA of Host Origin. (A) Left panels: *Cytb* PCR analysis of B16, B16ρ^0 and B16ρ^0SC and B16ρ^0SCL

tumor sub-lines from C57BL/6 (upper left panel) and NOD/scid mice (lower left panel). Right panels: *Cytb* PCR analysis of 4T1, 4T1ρ^0 and tumor sub-lines from orthotopic primary and metastatic tumors (upper right panel, 4T1ρ^0MFP, 4T1ρ^0MFPL) and s.c. primary and metastatic tumor (4T1ρ^0SC, 4T1ρ^0SCL) that form in Balb/c mice. (B) Left panels: sequence analysis of the polymorphic region (9817-9836 C57BL/6 reference NC_005089.1) of the mitochondrial *tRNA^{Arg}* gene from C57BL/6 and NOD/scid mice and from subcutaneous tumors derived from B16ρ^o cells grown in C57BL/6 and NOD/scid mice. Right panels: comparable sequence analysis of the mitochondrial *tRNA^{Arg}* gene from Balb/c mice and from a subcutaneous tumor derived from 4T1ρ^0 cells grown in Balb/c mice. A summary Table of the results is presented. (C) COI immunocytochemical staining (green) of parental, ρ^0 and individual sub-lines of B16 and 4T1 cells. Nuclei were stained with Hoechst 33342 (blue). Size bar, 10 μm.

Figure 3. Individual Cell Types Differ in Their Phenotype and Mitochondrial Morphology. (A) 4T1 and the derived sub-lines were evaluated using light microscopy. (B) The sub-lines were stained with EtBr and MitoTracker Red, and evaluated by confocal microscopy for yellow (EtBr) and red fluorescence (MitoTracker Red). Nuclei were stained with Hoechst 33342. The cells were evaluated using flow cytometry for the percentage of mitochondria with (upper right quadrant) and without (left quadrants) DNA. (C) The sub-lines were incubated with AO (red) to visualize acidic vacuoles and with Hoechst 33342 to show nuclei (blue). Cells were also probed by WB for LC3B-I/II, p62, Parkin and BNIP3 with actin as the loading control. Bafilomycin A treatment (20 μM, 16 h) was included in the LC3BII analysis to determine autophagic flux. (D) The

sub-lines were incubated with E-cadherin (green) and vimentin (red) and counterstained with Hoechst 33342 (blue), and inspected by confocal microscopy.

Figure 4. TEM Analysis of Individual Sub-lines Shows Mitochondrial Ultrastructural Differences. 4T1 cells and the derived sub-lines were grown on cover slips, processed for TEM as detailed in Materials and Methods, and examined using TEM. The bar indicates 500 nm for the general cell view and 200 nm for the magnified mitochondrial image. The lower graphs indicate percent mitochondria with visible cristae (left) and percent mitochondria with ring-like cristae (right) for each of the 4T1ρ^0 sub-lines. The percentage of mitochondria with visible cristae in 4T1 cells was set as 100%, the percentage of mitochondria with ring-like cristae in 4T1ρ^0 cells set as 100%. The data are derived from three independent experiments and the results expressed as mean values ± S.D. The symbol '*' documents significantly significant differences with $p<0.05$.

Figure 5. Bioenergetic Properties of 4T1 Cell Types. 4T1 cells and the derived sub-lines were assessed for glucose uptake (A), lactate production (B) and the level of ATP (C). Mitochondrial superoxide production was evaluated using MitoSOX (D), cytosolic hydrogen peroxide with DCF (E) and $\Delta\Psi_m$ using TMRM (F). (G) Cells were evaluated for routine, leak, net (R-L) and uncoupled (ETS) respiration using the Oxygraph respirometer as described in more detail in Materials and Methods and in the Legend to Figure S3A. (H) Cells were permeabilized with digitonin and evaluated for respiration at the presence of substrates specific for CI and CII. The data are derived from three independent experiments and the results expressed as mean values ± S.D. The symbol '*' documents significantly significant differences with $p<0.05$.

Figure 6. Mitochondrial DNA Content and Transcriptional Activity of 4T1 Cell Types. (A) 4T1, 4T1ρ^0 and tumor sub-lines were evaluated for the mtDNA:nDNA ratio using qPCR and specific primers (Supplementary Text). The analyses were performed using cells maintained in culture for a short period of time (1st analysis), 1 month (2nd analysis) and 4 months (3rd analysis). The sub-lines were also evaluated for the level of RC transcripts encoded by mtDNA (B) and nDNA (C) and for transcripts of mitochondrial regulatory genes (D) using qPCR and specific primers (Supplementary Text). The data are derived from three independent experiments and the results expressed as mean values ± S.D. The symbol '*' documents significantly significant differences with $p<0.05$.

Figure 7. Mitochondrial Protein Synthesis, Respiratory Complex Formation and Supercomplex Assembly in 4T1 Cell Types. (A) 4T1 cells and derived sub-lines were evaluated for newly synthesized proteins using the Clik-iT AHA kit. The sub-lines were also assessed for CS (B), SDH (C) and SQR activity (D) as detailed in Materials and Methods, as well as expression of specific proteins using WB and specific antibodies (E). Tubulin was used as a loading control. (F) The mitochondrial fraction was lysed in the presence of digitonin and subjected to NBGE. Specific subunits of individual complexes were detected using the antibodies as shown. HSP60 was used as a loading control. The level of expression of the individual bands representing RCs, subcomplexes and SCs, was evaluated by densitometry relative to HSP60. The data are derived from three independent experiments and the results expressed as mean values ± S.D. The symbol '*' documents significantly significant differences with $p<0.05$.

SUPPLEMENTARY TEXT

MATERIAL AND METHODS

Cell Culture, Tumor Formation and Establishment of Tumor-Derived Cells. B16 and 4T1 cells were grown in the IMDM and RPMI1640 medium, respectively, containing 10% FCS with 2 mM glutaMAX at 37ºC and 5% CO_2. To delete mtDNA, cells were cultured for 10-12 weeks with EtBr (50-100 ng/ml) supplemented with 1 mM pyruvate and 50 μg/ml uridine (King and Attardi, 1989). Loss of mtDNA was monitored by sensitivity to 2 μM FCCP (Herst and Berridge, 2007; Herst et al, 2011), PCR analysis of the mitochondrial *Cytb* gene and by pyruvate/uridine auxotrophy. B16 and B16ρ^0 cells ($2x10^5$) cells in HBSS were injected s.c. into the right flank of C57BL/6 or NOD/SCID mice. 4T1 and 4T1ρ^0 cells (10^5) were injected either subcutaneously into the right flank or into the mammary fat pad of female Balb/c mice. To determine the ability of parental and ρ^0 cells to seed and grow in the lung, 10^5 cells were injected intravenously.

Animal studies were performed according to the guidelines of the Australian and New Zealand Council for the Care and Use of Animals in Research and Teaching and were approved by the local Animal Ethics Committee.

Isolation of Mitochondria. Functional mitochondria were isolated as described (Schmitt et al, 2013). In brief, cells were homogenized in the isolation buffer containing 200 mM sucrose, 10 mM Tris-MOPS and 1 mM EGTA/Tris using the Balch homogenizer (Isobiotec) coupled to high-precision New Era NE-1010 pump system. Cell suspension containing 40-50 x 10^6 cells in 5 ml was passed 3 times through a 10 μm wide opening using a 5 ml syringe at 0.5 ml/min. The homogenate was centrifuged at 800 x *g* for 8 min at 4°C, and the supernatant containing mitochondria was further centrifuged for 15 min at

10,000 x *g*. Peletted mitochondria were re-suspended in 100-200 μl of the isolation buffer, and 50-100 μl of the suspension was immediately used for respiration evaluation.

Sequence Analysis of Mitochondrial *tRNA^{Arg}* Gene. Total DNA was obtained from cells or isolated mitochondria using the Quick-gDNA^{TM} MiniPrep kit (Zymo Research) according to the manufacturer's instructions. A 483 bp tRNA R region containing the polymorphic locus (position 9821 of reference sequence NC_005089.1) was amplified by PCR using a forward primer (5'-TCG ACC CTA CAA GCT CTG CAC GT-3') and reverse primer (5'-TGG TGA TGG GGA TTG GTA TGG AGC-3'). PCR was performed in 20 μl reaction volumes containing 500 ng sample DNA, 0.5 μM of each primer and iTaq DNA Polymerase, dNTP mixture and PCR buffer (Intron Biotechnology). The reaction conditions were: 94^{o}C for 2 min, 35 cycles of 94^{o}C for 20 s; 70^{o}C for 10 s; 72^{o}C for 30 s, and then 72^{o}C for 5 min. PCR products were analyzed by 2% agarose gel electrophoresis and purified using UltraClean PCR Clean-Up Kit (Mo Bio Labs). Sequencing was performed by the Massey University Genome Service using a capillary ABI3730 Genetic Analyzer (Applied Biosystems). The *tRNA^{arg}* gene polymorphic region of B16 and 4T1 cells was sequenced 8-9 times using both forward and reverse primers on multiple occasions over 13-14 months, while isolated mtDNA from C57BL/6, Balb/c and NOD/SCID mice was sequenced at least once with both forward and reverse primers to confirm published results (Bayona-Bafaluy et al., 2003). With cells grown in culture from tumors that grew from B16ρ^0 and 4T1ρ^0 cells the polymorphic region was sequenced 2-3 times using both forward and reverse primers on each occasion.

Microscopic and Flow Cytometric Cell Evaluation. For COI evaluation, **c**ells were fixed with 4% formalin, permeabilized with 0.2% Triton X-100 and incubated for 1 h with monoclonal anti-COI IgG (Molecular Probes) followed by anti-mouse AlexaFluor

488 IgG (Molecular Probes) for 1 h. DAPI was used for nuclear staining. For vimentin and E-cadherin staining, fixed and permeabilized cells were incubated overnight with 4 μg/ml mouse monoclonal anti-vimentin IgG (Santa Cruz) and 1 μg/ml rabbit polyclonal anti-E-cadherin IgG (Sigma-Aldrich) and for 3 h with anti-mouse-AlexaFluor 594 IgG and anti-rabbit-AlexaFluor 488 IgG (Molecular Probes), and stained with 1 μg/ml Hoechst 33342 (Sigma-Aldrich) to visualize nuclei. For live cell imaging of mitochondria and mtDNA, cells were grown in chamber slides (LabTek) and incubated for 30 min with 100 nM MitoTracker Red (Molecular Probes) and 5 μg/ml Hoechst 33342, and subsequently for 4 min with 2 μg/ml EtBr. Images were captured and analyzed using the FV1000 confocal microscope and Fluoview software (Olympus). For flow cytometric quantification of mtDNA content, cultured cells were stained as above without nuclear staining. Mean fluorescence readings were acquired using the FACScalibur cytometer (BD Biosciences) and the percentage of gated cells analyzed using the FlowJo software version 7.6.5 (Treestar). TEM was accomplished as follows. Cells were grown on cover-slips, fixed with 2% glutaraldehyde (Agar Scientific) and post-fixed with 1% OsO_4 made up in Sorensen's phosphate buffer (0.1 M, pH 7.2-7.4), dehydrated, and embedded in Epon-Durkupan (Sigma-Aldrich). Ultrathin sections (~70-90 nm) were cut, contrasted with uranyl acetate (Agar Scientific), and examined in the Morgagni 268 transmission electron microscope (FEI) at 80 kV and in the TECNAI G2 20 LaB6 electron microscope (FEI) at 200 kV. Images were captured with Mega View III CCD camera (Olympus Soft Imaging Solutions). For statistical evaluation, 50 mitochondria per cell in 25 cells from each sub-line were inspected and scored for mitochondria with clearly visible cristae, suggestive of functional mitochondria and mitochondria with ring-like cristae, suggestive of dysfunctional mitochondria.

Evaluation of $\Delta\Psi_m$ and ROS. The $\Delta\Psi_m$-sensitive fluorescent probe TMRM was utilized, and the cells evaluated by flow cytometry. The mitochondrial uncoupler FCCP was used as a control to determine non-specific TMRM loading. Cellular ROS were evaluated using the probes DCF-DA or MitoSOX. Cells were incubated with either probe for 10 min under normal culture conditions, harvested and fluorescence of the oxidized probes assessed by flow cytometry. All probes were from Sigma-Aldrich, MitoSOX from Molecular Probes.

Glucose Uptake, ATP Generation and Lactate Assays. For glucose uptake, cells were pre-incubated in low-glucose (1 g/l) DMEM for 24 h at 37°C and 5% CO_2, followed by 15-min incubation in normal DMEM (4.5 g/l glucose) in the presence of 50 μM 2-nitrobenzodeoxyglucose (2-NBDG; Life Technologies); glucose uptake was then analyzed by flow cytometry. For ATP evaluation, cells were seeded at 10^5 per well in 96-well plates and intracellular levels of ATP determined using a luciferase-based assay (CellTiter-Glo® Luminescent Assay, Promega). Results were normalized to the total protein level in the cell lysate assessed in each well determined by the BCA assay. For lactate evaluation, cells were seeded at 10^5 per well in 96-well plates. Aliquots of the medium were used for the analysis of lactate using a colorimetric kit (Trinity Biotech) following 24 h incubation. Results were normalized to the total protein level in the cell lysate.

Respiration Assays. Experiments evaluating intact cell respiration were performed with cells suspended in RPMI medium without serum. Oxygen consumption was evaluated for cellular ROUTINE respiration, oligomycin-inhibited LEAK respiration, FCCP-stimulated uncoupled respiration (ETS) and rotenone/antimycin-inhibited residual respiration (ROX). Respiration via mitochondrial complexes was evaluated using digitonin-

permeabilized cells suspended in the mitochondrial respiration medium MiR06, and oxygen consumption was evaluated for routine respiration, CI-linked respiration, (CI+CII)-linked respiration, maximum uncoupled respiration, CII-linked uncoupled respiration as well as residual oxygen consumption. Respiration via CI and CII was evaluated in the presence of the proper substrates and inhibitors of the other complex. The results were related to the number of cells. Detailed description of the conditions is in the Legend to Supplementary Figures.

mtDNA Level Assay. Total DNA was extracted using the AquaPure Genomic DNA Isolation Kit (BioRad). 50 ng of DNA was diluted with water to 4.5 μl, and 0.5 μl of the combined 10 μM forward and reverse primers added (for mtDNA, mMito1 primers for nDNA mB2M1 primers; see Supplementary Text for sequences) and 5 μl of 2xRT² SYBR® Green qPCR Mastermix (Qiagen) added. The reaction was run on the Eco qPCR System (Illumina) with the following setting: one cycle of 50°C for 2 min; one cycle of 95°C for 10 min; 40 cycles of 95°C for 15 s and 60°C for 1 min.

PCR Analysis of Mitochondrial *Cytb* Gene. DNA was purified from 10^6 cells using the Quick-gDNA™ MiniPrep (Zymo Research), and each sample analyzed by PCR using the *Cytb* gene as a mtDNA marker with forward primer (5'-TCC TTC ATG TCG GAC GAG GCT-3') and reverse primer (5'-ACG ATT GCT AGG GCC GCG AAT-3'). PCR was carried out in a BioRad iCycler for 30 cycles of 20 s at 94ºC, 20 s at 58ºC and 30 s at 72ºC, and analyzed by 2% agarose gel electrophoresis.

qPCR of mtDNA- and nDNA-Coded Genes. RNA was obtained in triplicate from 4T1- and 4T1ρ^0- derived sub-lines using the RNeasy Mini Kit (Qiagen). The Revertaid First-Strand Synthesis System plus random hexamer primers (Fermentas) were used to reverse-transcribe total RNA into cDNA. Primers specific for all mitochondrial and nuclear

encoded genes (see Supplementary Text for sequences of primers) were then assessed with 2x EvaGreen (Solis BioDyne) using the Eco qPCR System. Target genes were normalized to the housekeeping gene GAPDH, and change in gene expression was determined using the ΔΔCt method.

mtDNA isolation and sequencing. DNA was isolated from cell pellets according to manufacturer's instructions using the DNAzol product (MRC). Briefly, cells were lysed in 1 ml of DNAzol, spun at 2,000 x *g* for 5 min, and the resulting supernatant precipitated with 0.5 ml of EtOH, spun at 14,000 x *g* for 10 min, and washed twice with 75% ethanol. the resulting pellet was air-dried and dissolved in 8 mM NaOH. The DNA preparation containing nDNA and mtDNA was quantified by Nanodrop and further amplified using mtDNA-specific primers and PCR. The full length mtDNA was covered by amplifying and sequencing ten 1.8 kb long dsDNA PCR products. PCR products were run on an agarose gel to confirm the specificity of the reaction and were purified using the DNA clean-and-concentrator kit (Zymoresearch). 200 to 400 ng of the purified products was combined with water and 0.5 µl of 100 µM primer stocks to yield 10 µl sequencing reaction mixture. Sequencing was performed by the GACT Biotech by the classical Sanger sequencing, and the resulting sequences aligned using the SeqManPro suite from the DNASTAR Lasergene 11 software.

Native Blue Gel Eletrophoresis (NBGE). NBGE was accomplished basically as published (Wittig et al., 2006). In brief, mitochondria were isolated using a standard protocol. Digitonin-solublized mitochondria were separated on NativePAGE Novex Bis-Tris 3-12% gradient gels for CI and 4-16% gradient gels for CII, CIII, CIV and CV. After electrophoresis, the gels were incubated in the SDS-PAGE running buffer for 5 min and proteins transferred to PVDF membranes probed with specific antibodies against

complex I (NUDFA9), CII (SDHA or SDHB), CIII (CORE2), CIV (COVa) and CV (ATPaseβ) and HSP60 as the loading control.

Western Blotting. Cells were lysed in the RIPA buffer supplemented with the Complete Protease Inhibitor Cocktail (Roche). The lysate was cleared by centrifugation and total protein determined. 40 μg of total protein were resolved by SDS-PAGE and transferred to nitrocellulose membranes, which were then probed with appropriate antibodies (NDUFS3, NDUFA9, SDHA, SDHB, Core2, COI, COIV, ATPaseβ, PGCα, TIM23, VDAC, OPA1, Parkin, BNIP3 and HSP60 were from Abcam, SDHFA2 from Santa Cruz, SOD2 from Acris Antibodies, Cyt c from BD Pharmingen, LC3BI/II form Cell Signaling, tubulin from Exbio, and actin from Sigma-Aldrich). The blotted proteins reacted with specific antibodies were detected using the ECL Western Blotting Substrate (Pierce).

***In vitro* Translation of mtDNA-Encoded Genes**. Newly synthesized mtDNA-encoded proteins were evaluated in intact cells using the Clik-iT AHA kit (Invitrogen). Briefly, cells were incubated with methionine-free RPMI for 10 min at 37°C and 5% CO_2 and subsequently with 100 μg/ml cyclohexamide. After 30 min, 3 mM L-azidohomoalanine (azhal, a methionine analog) was added and the cells incubated for 2 h. Azhal-labeled cells were harvested and the total cellular protein extracted in 20 mM Tris-HCl pH 8.0, 1% SDS and 250 U/ml benzonase nuclease (Sigma-Aldrich). The cyclo-addition of alkyne-tagged TAMRA to azhal-labeled proteins was carried out according to the manufacturer's protocol. Proteins were separated by Tris-Tricine SDS-PAGE and transferred to a PVDF membrane, and mitochondrial translation products detected with anti-TAMRA IgG (Abcam). Total protein stained with Commassie Blue was used as a loading control.

CS, SDH and SQR Activity Assays. CS activity was assessed by the reduction of 5,5′-dithiobis-(2-nitrobenzoic acid) (DTNB) using the coupled reaction with acetyl-CoA and oxaloacetate. In brief, 10 μg of protein lysate were added to 10 μM DTNB and 30 μM acetyl-CoA and the reaction initiated by adding 10 μM oxaloacetate in a 200 μl reaction mixture. The change in absorbance of DTNB was assessed spectrophotometrically for 90 s at 412 nm and 30ºC, and the activity calculated as described (Shephard and Garland, 1969). Purified CS was used as positive control. For SQR activity, 40 μg of protein lysate extracted before the assay (Cell Lysis Buffer, Cell Signaling) were added to 1 ml of the SQR assay buffer (10 mM KH_2PO_4, pH 7.8, 2 mM EDTA, 1 mg/ml BSA), 80 μM DCPIP, 4 μM rotenone, 0.2 mM ATP and10 mM succinate, and incubated at 30ºC for 10 min. Decylubiquinone was added to a final concentration of 80 μM, and absorbance assessed every minute for 30 min at 600 nm (Barrientos et al., 2009). SDH activity was assessed as described (Dong et al., 2008).

Primers Used for qPCR Analysis of mtDNA- and nDNA-Coded Genes

Gene	Forward	Reverse
mMito1	CTA GAA ACC CCG AAA CCA AA	CCA GCT ATC ACC AAG CTC GT
mB2M1	ATG GGA AGC CGA ACA TAC TG	CAG TCT CAG TGG GGG TGA AT
D-Loop	AGG TTT GGT CCT GGC CTT AT	GTG GCT AGG CAA GGT GTC TT
12S	CTA GCC ACA CCC CCA CGG GA	CGT ATG ACC GCG GTG GCT GG
16S	CGG CAA ACA AGA ACC CCG CC	GTC AGG ATA CCG CGG CCG TT
Nd1	CAG CCG GCC CAT TCG CGT TA	AGC GGA AGC GTG GAT AGG ATG C
Nd2	TCC TCC TGG CCA TCG TAC TCA ACT	AGA AGT GGA ATG GGG CGA GGC
Nd3	ACC CTA CAA GCT CTG CAC GCC	GCT CAT GGT AGT GGA AGT AGA AGG GCA

Nd4	TCG CCT ACT CCT CAG TTA GCC ACA	TGA TGA TGT GAG GCC ATG TGC GA
Nd4l	TCG CTC CCA CCT AAT ATC CAC ATT GC	GCA GGC TGC GAA AAC CAA GAT GG
Nd5	TCG GAA GCC TCG CCC TCA CA	AGT AGG GCT CAG GCG TTG GTG T
Nd6	AAT ACC CGC AAA CAA AGA TCA CCC AG	TGT TGG GGT TAT GTT AGA GGG AGG GA
Ndufs3	TGG CAG CAC GTA AGA AGG G	CTT GGG TAA GAT TTC AGC CAC AT
Sdha	GGA ACA CTC CAA AAA CAG ACC T	CCA CCA CTG GGT ATT GAG TAG AA
Sdhb	AAT TTG CCA TTT ACC GAT GGG A	AGC ATC CAA CAC CAT AGG TCC
Sdhc	GTT CTT GCT GAG ACA TGT CA	AGT GAG TGG TAC ATG AGC
Sdhd	TGG TCA GAC CCG CTT ATG TG	GGT CCA GTG GAG AGA TGC AG
Cytb	ACA CGC AAA CGG AGC CTC AA	TGC TGT GGC TAT GAC TGC GAA CA
Uqcrc2	AAA GTT GCC CCG AAG GTT AAA	GAG CAT AGT TTT CCA GAG AAG CA
mt-Co1	CCA GTG CTA GCC GCA GGC AT	TCT GGG TGC CCA AAG AAT CAG AAC A
mt-Co2	AGT TGA TAA CCG AGT CGT TCT GCC A	TCG GCC TGG GAT GGC ATC AGT
mt-Co3	ACC TAC CAA GGC CAC CAC ACT CC	GCA GCC TCC TAG ATC ATG TGT TGG T
mt-CO4	ATT GGC AAG AGA GCC ATT TCT AC	CAC GCC GAT CAG CGT AAG T
Atp6	GCT CAC TCG CCC ACT TCC TTC C	GCC GGA CTG CTA ATG CCA TTG GTT
Atp8	ATG CCA CAA CTA GAT ACA TCA ACA	GGG GTA ATG AAT GAG GCA AA
Atp5b	GGT TCA TCC TGC CAG AGA CTA	AAT CCC TCA TCG AAC TGG ACG
Top1m	GGG ATT CCA AGA TCC CTG AC	ATC TTG TCC ACA ACC CCC TT
Nrf1	ACT CAG CCA CGT TGG ATG	GAG GCG GCA GCT CTG AAT TA
Nrf2	ATG ATG GAC TTG GAG TTG CCA	GCT CAT AGT CCT TCT GTC GC
Tfam	GGC AAA GGA TGA TTC GGC TC	CAC TTC GTC CAA CTT CAG CC
Tfb1m	GAC TGC GAG CGG TGA AAC AG	CCT GGG ATA AAG CGA GTG T
Tfb2m	GCC AAT TGC TTG CAT CTC CC	ACA AGG CCT GGG ACT TAT GC
Scaf1	GCA GAA GTT TTT CA GAA GGC T	GGG CGA TCA GGC AGT AGA TG

Hig2a	CCC CAG TTA TCG AGG GCT TC	CCG TCC CCA GAC AGC CTA T
Gapdh	ACA GCC GCA TCT TCT TGT GCA GTG	GGC CTT GAC TGT GCC GTT GAA TTT

LEGEND TO SUPPLEMENTARY FIGURES

Figure S1. Tumor-forming Ability of 4T1ρ^0 Cells

4T1ρ^0 cells (10^5, 10^4,10^3,10^2) were injected s.c. into groups of 5 Balb/c mice and tumor growth monitored every 2 days.

Figure S2. 'Matching' 4T1 Tumor Cells Do Not Differ in Morphology

(A) 4T1, 4T1SC and 4T1SCL cells were grown to 70% confluency, stained with EtBr and MitoTracker Red, and inspected by confocal microscopy showing the individual channels as well as their overlay (including nuclear staining with Hoechst 33342). Cells stained in a corresponding manner with EtBr and MitoTracker Red were evaluated using flow cytometry to reveal the percentage of mitochondria with and without DNA. (B) Cells were subjected to TEM and inspected for mitochondrial morphology.

Figure S3. 'Matching' Tumor Cells Show Similar Characteristics Relating to Their Mitochondrial Function. 4T1, 4T1SC and 4T1SCL cells were grown and assessed, as detailed in Materials and Methods, for glucose uptake (A), lactate release (B), ATP generation (C), ROS generation using the MitoSOX (D) and DCF (E) probe, routine respiration using the Oxygraph (F), mtDNA:nDNA ratio by qPCR (G), expression of

mitochondria regulatory genes by qPCR (H), CS (I), SDH (J) and SQR activities (K), and protein expression using WB (L).

Figure S4. Mitochondrial ROS Production by Tumor Cells Derived from Mitochondrially-Defective ρ^0 Cells. (A) Mitochondrial oxidant production by 4T1 and 4T1ρ^0 cells, and 6TG-resistant cells from primary subcutaneous (4T1ρ^0SC) and orthotopic (4T1ρ^0MFP) tumors that grew from 4T1ρ^0 cells, and from lung metastases (4T1ρ^0SCL and 4T1ρ^0MFPL) from these primary tumors (left 6 panels), and (B) by B16 and B16ρ^0 cells and cells from primary subcutaneous (B16ρ^0SC) and lung metastases (B16ρ^0SCL (right panels) used MitoSOX staining.

Figure S5. Primary Data on Mitochondrial Respiration in 4T1 Cell Lines

(A) 4T1, 4T1ρ^0, 4T1ρ^0SC, 4T1ρ^0CTC and 4T1ρ^0SCL cells were plated and, when reaching 50-70% confluency, harvested and evaluated for routine (R), leak (L), net (R-L) and uncoupled (E) and residual (ROX) respiration using the Oxygraph respiratometer as described in more detail in Materials and Methods. (B) 4T1, 4T1ρ^0SC, 4T1ρ^0CTC and 4T1ρ^0SCL cells were plated and, when reaching 50-70% confluency harvested, permeabilized with digitonin and evaluated for respiration at the presence of substrates specific for CI and CII using the protocol indicated in more detail in Materials and Methods. The lower panels document representative evaluations of the respiration curves, indicating the 'leak', respiration via CI, CI+CII, uncoupled respiration via CI+CII (ETC) plus uncoupled respiration via CII. The residual respiration (ROX) was set to zero. The abbreviations in the top left line graphs in panels A and B are: Omy, 0.5 μM oligomycin;

F1, 1 μM FCCP; Rot, 0.1-0.5 μM rotenone; Dig, 10 μg digitonine per 10^6 cells; PMG, 5 mM pyruvate; 2 mM malate; 10 mM glutamate; ADP, 1-5 μM ADP; cyt c, 10 μM Cyt c; succ, 10 mM. (C) Mitochondria isolated from individual 4T1 sub-lines were assessed for respiration as mentioned above for permeabilized cells.

Figure 1

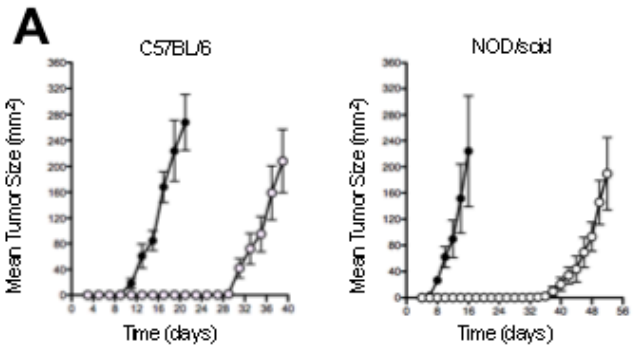

Tumor (NOD/scid)	Days after iv injection	Lung nodules (Mean ± SD)	Lung Weighting (Mean ± SD)
none	0	0	157 ± 27
B16	21	126 ± 39	674 ± 124
B16ρ°	21	0	182 ± 22
B16ρ°	64	0	181 ± 45
B16ρ°SC	21	84 ± 42	468 ± 118***
B16ρ°SCL	21	102 ± 26	553 ± 112***

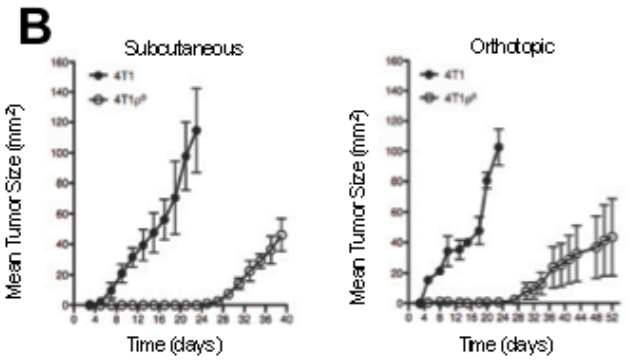

Tumor (Balb/c)	Days after iv injection	Lung nodules (Mean ± SD)	Lung Weighting (Mean ± SD)
none	0	0	201 ± 22
4T1	21	103 ± 14	449 ± 62
4T1ρ°	21	0	223 ± 31
4T1ρ°	64	0	192 ± 16
4T1ρ°SC	21	78 ± 56	311 ± 102*
4T1ρ°SCL	21	93 ± 44	401 ± 76***

4T1 4T1ρ° 4T1ρ°MFPL 4T1ρ°SC 4T1ρ°SCL

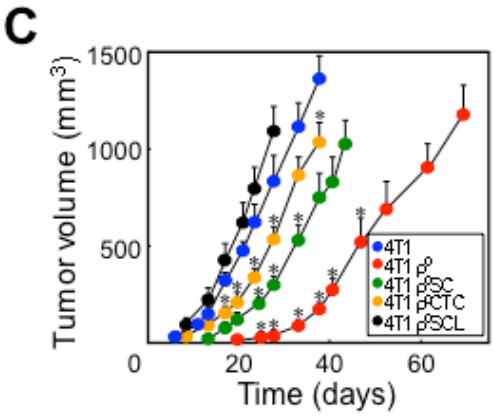

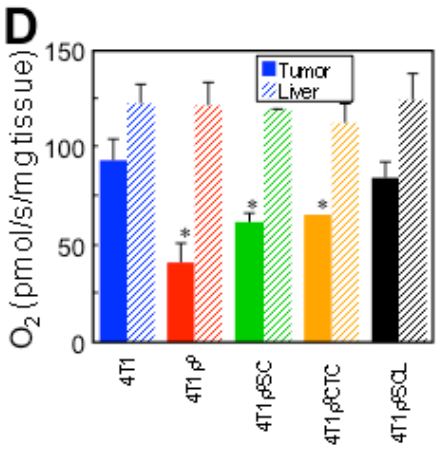

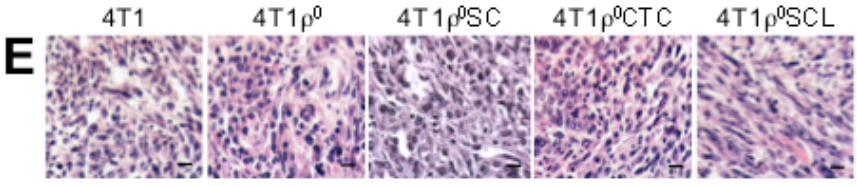

Figure 2

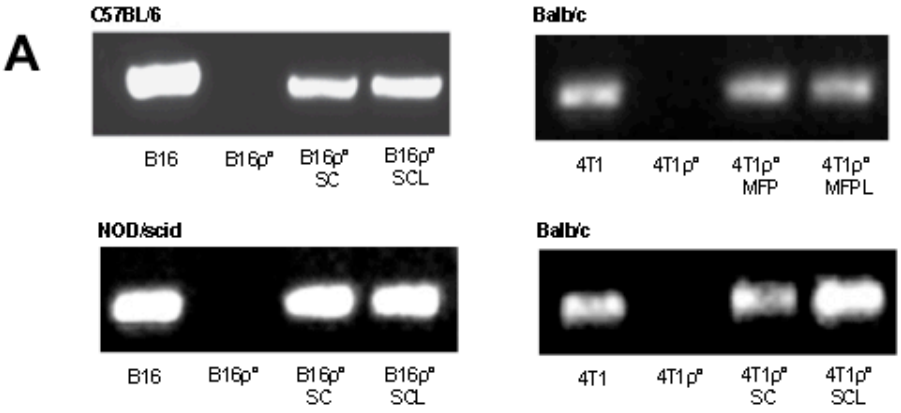

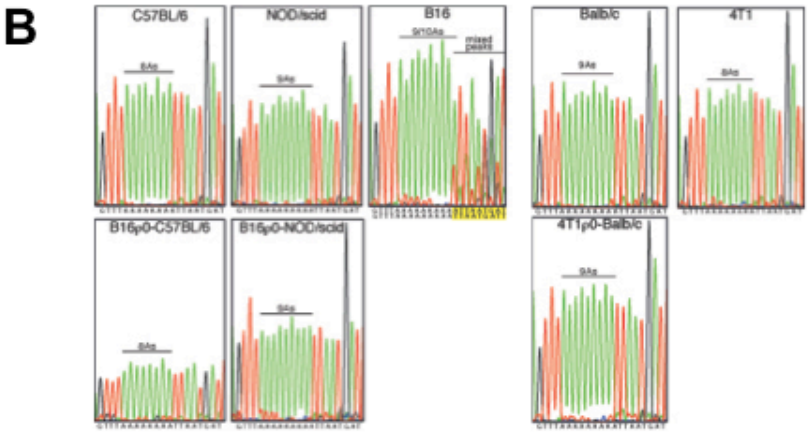

Mouse strain or tumor	Polymorphic $tRNA^{Arg}$ locus	Mouse strain or tumor	Polymorphic $tRNA^{Arg}$ locus
C57BL/6	8A	Balb/c	9A
B16ρ°SC (C57BL/6)	8A	4T1ρ°SC (Balb/c)	9A
B16	9/10A	4T1	8A
NOD/scid	9A		
B16ρ°SC (NOD/scid)	9A		

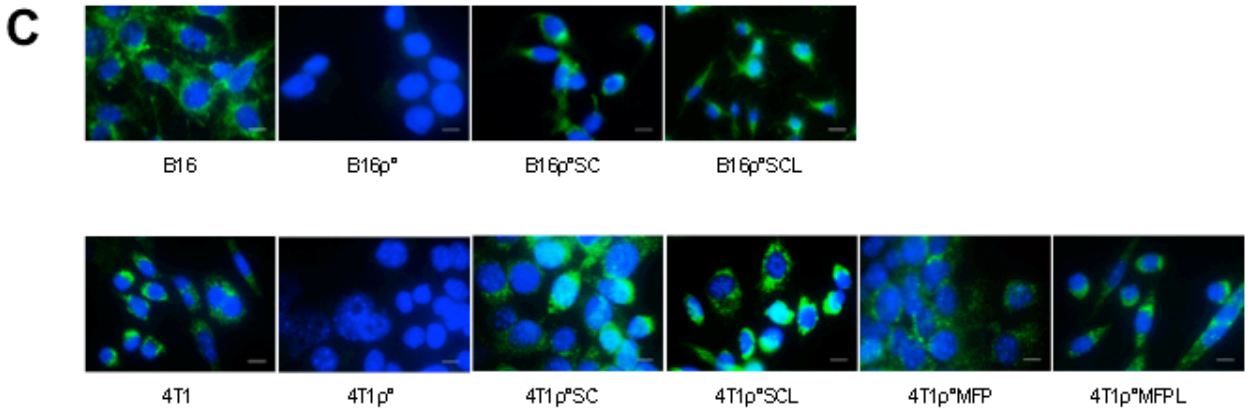

Figure 3

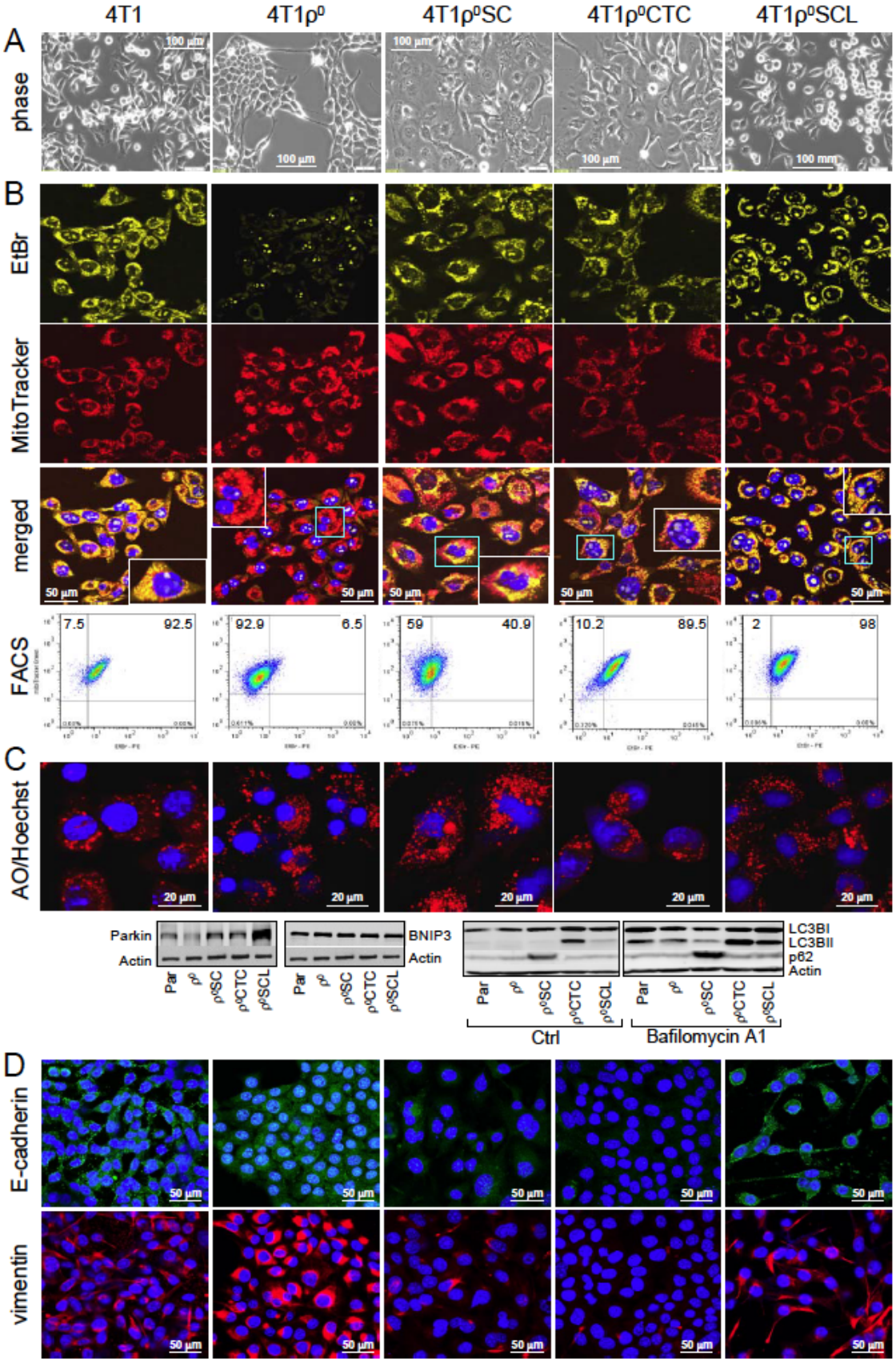
4T1
4T1ρ⁰
4T1ρ⁰SC
4T1ρ⁰CTC
4T1ρ⁰SCL
A
phase
B
EtBr
MitoTracker
merged
FACS
7.5
92.5
92.9
6.5
59
40.9
10.2
89.5
2
98
C
AO/Hoechst
Parkin
Actin
BNIP3
Actin
LC3BI
LC3BII
p62
Actin
Par
ρ⁰
ρ⁰SC
ρ⁰CTC
ρ⁰SCL
Ctrl
Bafilomycin A1
D
E-cadherin
vimentin
50 μm
20 μm
100 μm

Figure 4

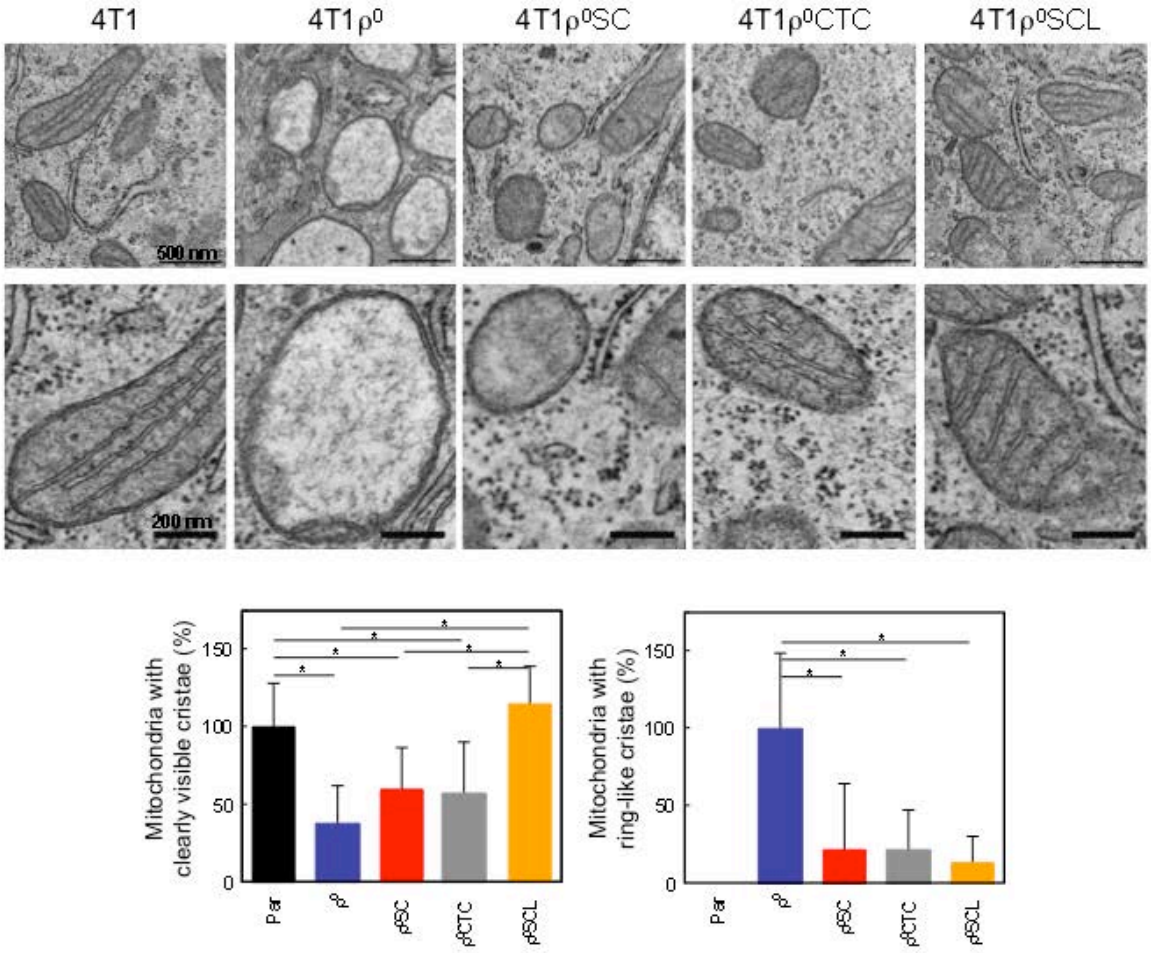
4T1
4T1ρ0
4T1ρ0SC
4T1ρ0CTC
4T1ρ0SCL
500 nm
200 nm
Mitochondria with clearly visible cristae (%)
150
100
50
0
Par
ρ0
ρSC
ρCTC
ρSCL
Mitochondria with ring-like cristae (%)
150
100
50
0
Par
ρ0
ρSC
ρCTC
ρSCL

Figure 5

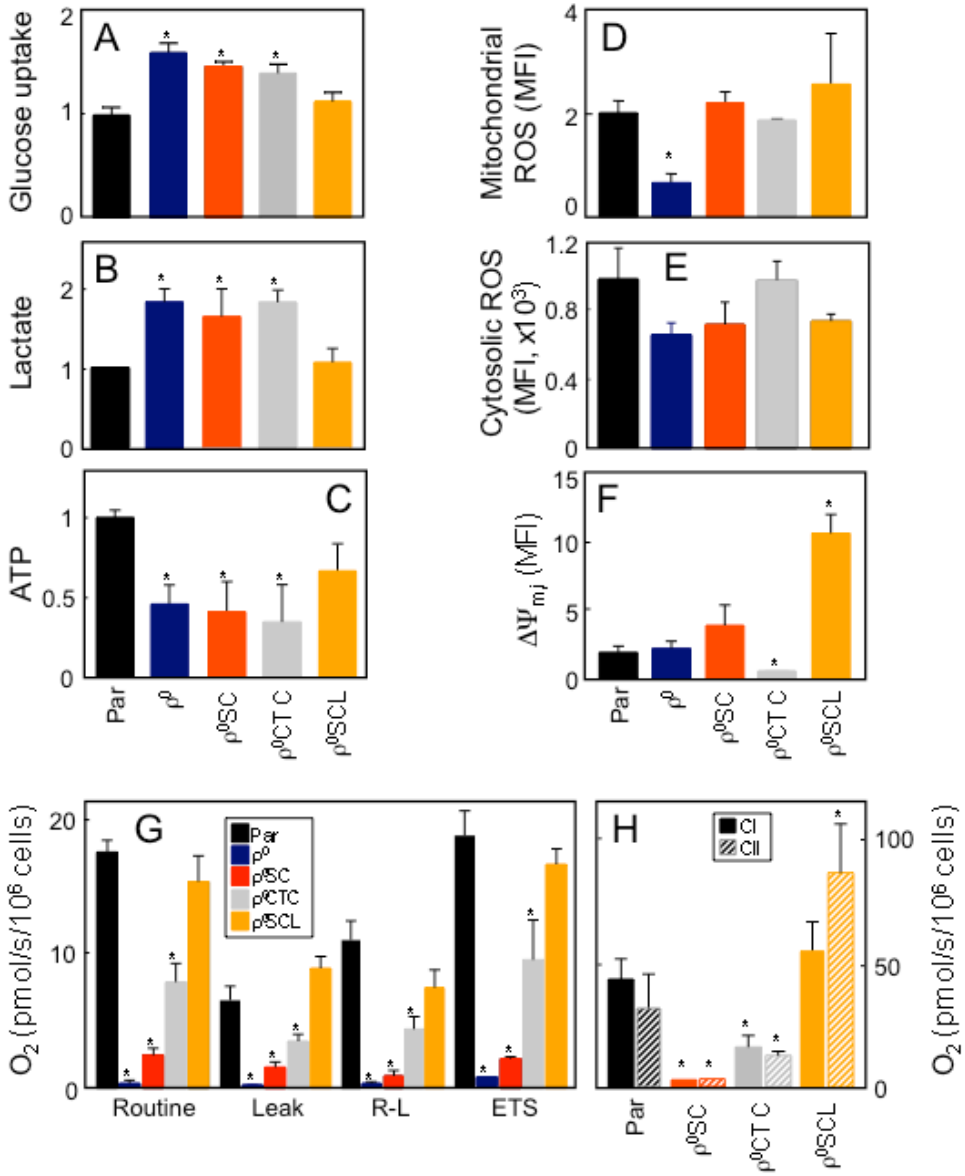
A
Glucose uptake
B
Lactate
C
ATP
D
Mitochondrial ROS (MFI)
E
Cytosolic ROS (MFI, x10³)
F
ΔΨmj (MFI)
Par
ρ⁰
ρ⁰SC
ρ⁰CTC
ρ⁰SCL
G
O2 (pmol/s/10⁶ cells)
Routine
Leak
R-L
ETS
H
CI
CII

Figure 6

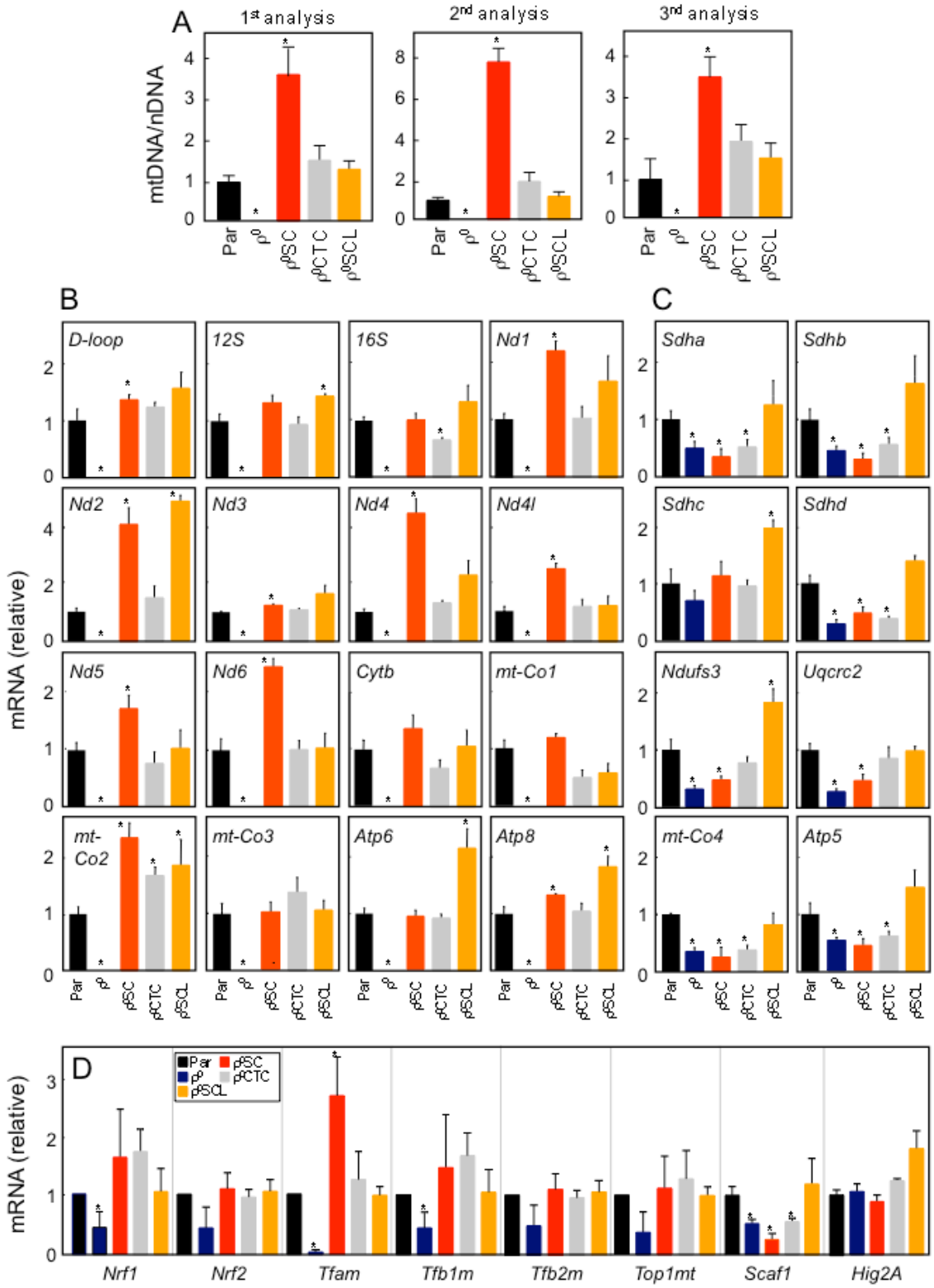
A
1st analysis
2nd analysis
3nd analysis
mtDNA/nDNA
Par
ρ0
ρ0SC
ρ0CTC
ρ0SCL
B
C
D-loop
12S
16S
Nd1
Sdha
Sdhb
Nd2
Nd3
Nd4
Nd4l
Sdhc
Sdhd
Nd5
Nd6
Cytb
mt-Co1
Ndufs3
Uqcrc2
mt-Co2
mt-Co3
Atp6
Atp8
mt-Co4
Atp5
mRNA (relative)
ρSC
ρCTC
ρSCL
Nrf1
Nrf2
Tfam
Tfb1m
Tfb2m
Top1mt
Scaf1
Hig2A

Figure 7

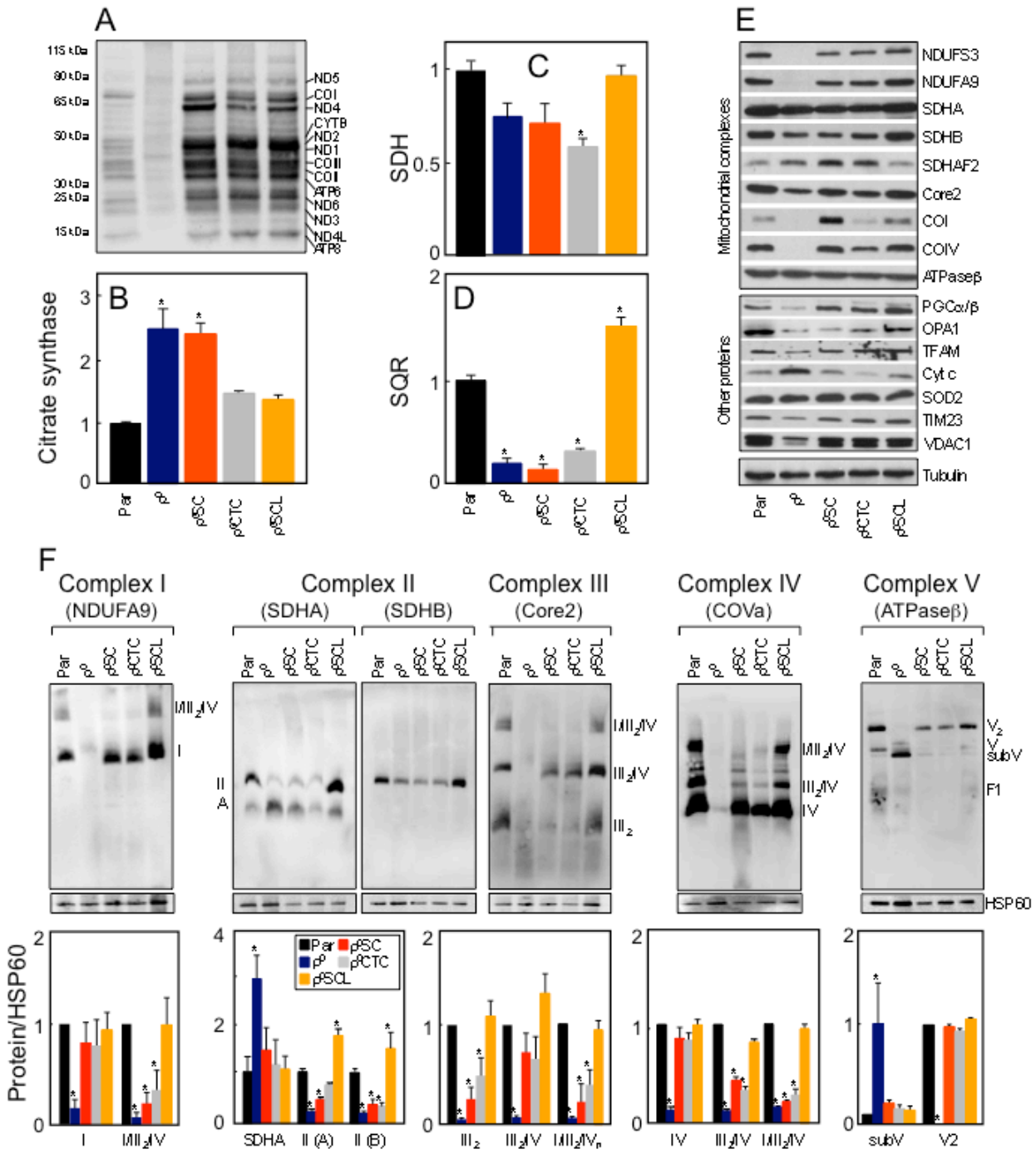
A
B
C
D
E
F
Citrate synthase
SDH
SQR
Mitochondrial complexes
Other proteins
NDUFS3
NDUFA9
SDHA
SDHB
SDHAF2
Core2
COI
COIV
ATPaseβ
PGCα/β
OPA1
TFAM
Cyt c
SOD2
TIM23
VDAC1
Tubulin
Par
ρ0
ρSC
ρCTC
ρSCL
Complex I
(NDUFA9)
Complex II
(SDHA)
(SDHB)
Complex III
(Core2)
Complex IV
(COVa)
Complex V
(ATPaseβ)
HSP60
Protein/HSP60
SDHA
II (A)
II (B)
IV
subV
V2

Figure S1

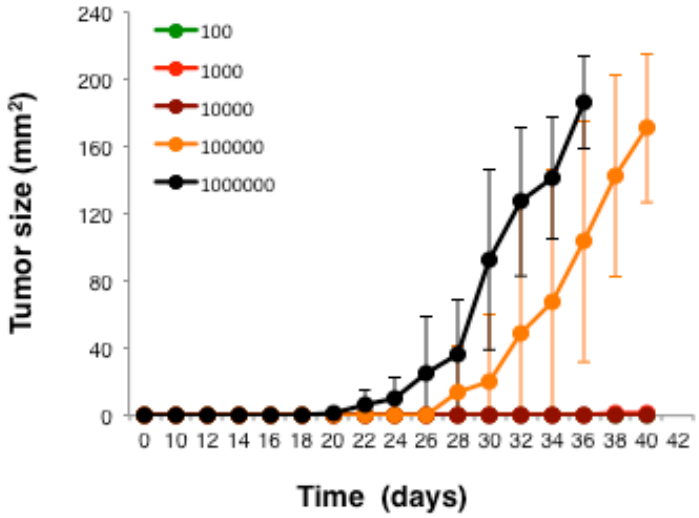
240
200
160
120
80
40
0
100
1000
10000
100000
1000000
Tumor size (mm²)
0 10 12 14 16 18 20 22 24 26 28 30 32 34 36 38 40 42
Time (days)

Figure S2

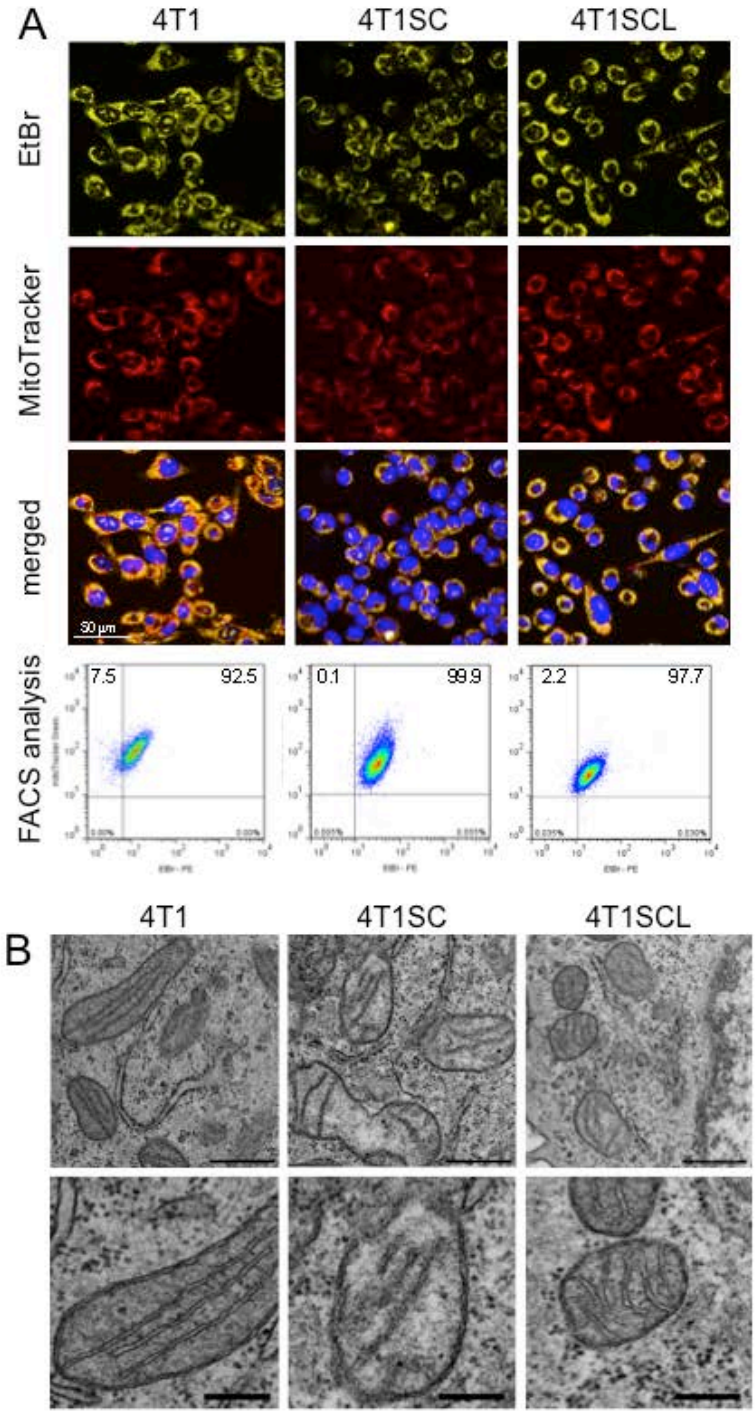
A
4T1
4T1SC
4T1SCL
EtBr
MitoTracker
merged
50 µm
FACS analysis
7.5
92.5
0.1
99.9
2.2
97.7
B
4T1
4T1SC
4T1SCL

Figure S3

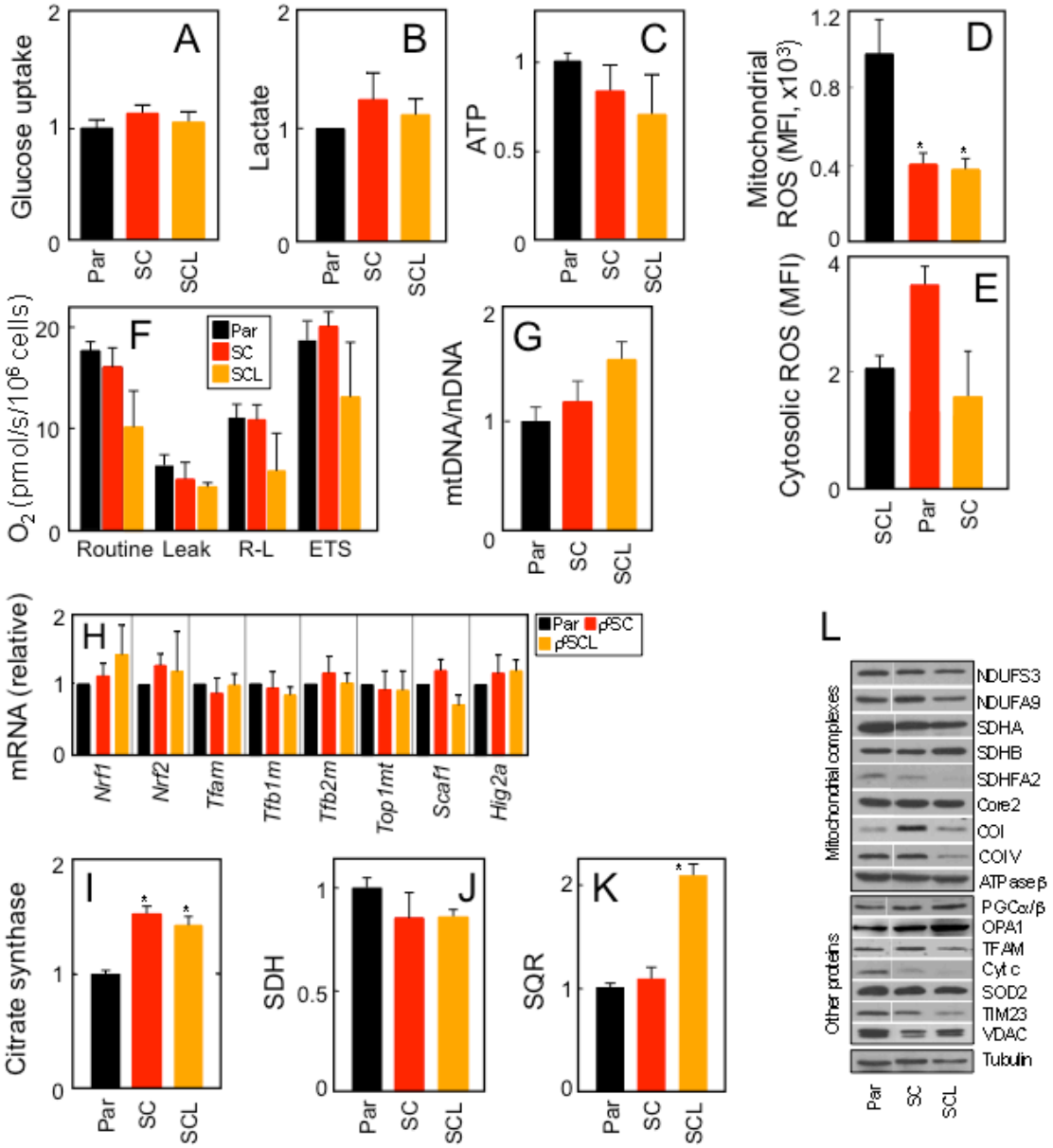
A
Glucose uptake
B
Lactate
C
ATP
D
Mitochondrial ROS (MFI, x10³)
E
Cytosolic ROS (MFI)
F
O2 (pmol/s/10⁶ cells)
Routine
Leak
R-L
ETS
G
mtDNA/nDNA
H
mRNA (relative)
Nrf1
Nrf2
Tfam
Tfb1m
Tfb2m
Top1mt
Scaf1
Hlg2a
Par
ρSC
ρSCL
I
Citrate synthase
J
SDH
K
SQR
L
Mitochondrial complexes
NDUFS3
NDUFA9
SDHA
SDHB
SDHFA2
Core2
COI
COIV
ATPaseβ
Other proteins
PGCα/β
OPA1
TFAM
Cyt c
SOD2
TIM23
VDAC
Tubulin

Figure S4

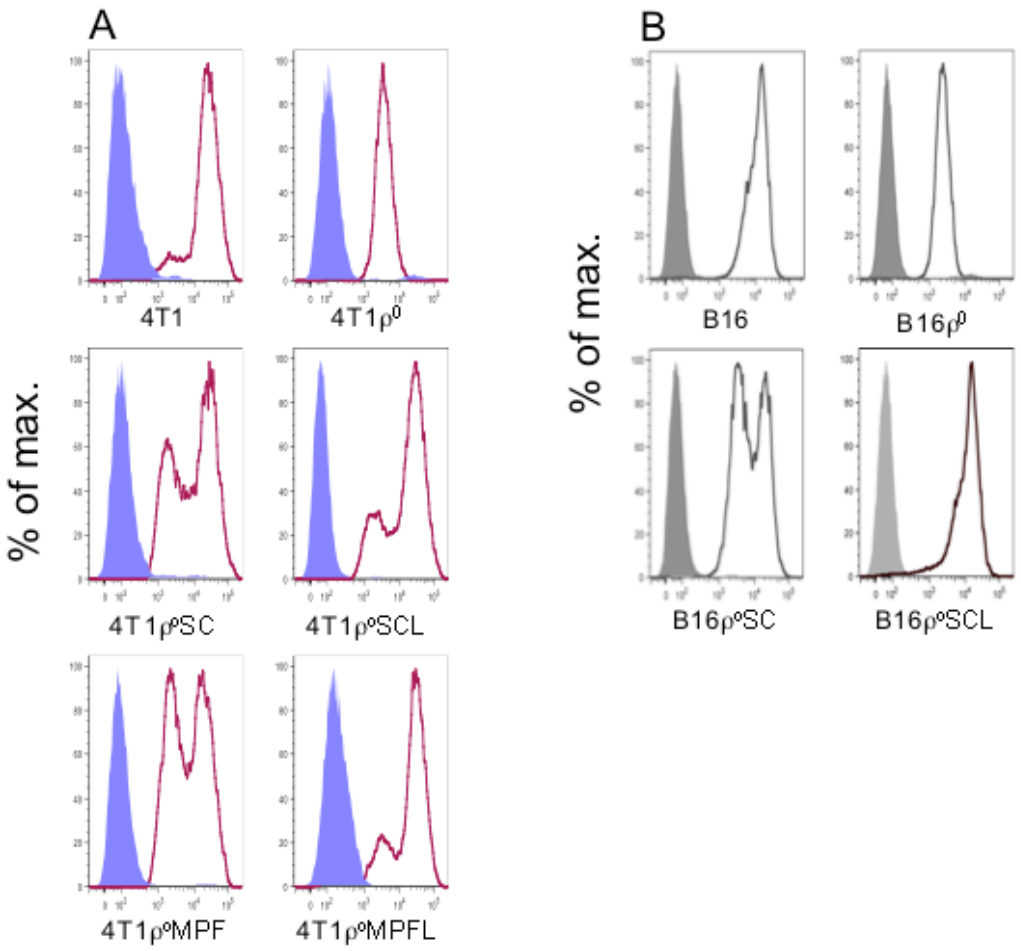
A
B
% of max.
% of max.
4T1
4T1ρ0
4T1ρºSC
4T1ρºSCL
4T1ρºMPF
4T1ρºMPFL
B16
B16ρ0
B16ρºSC
B16ρºSCL

Figure S5

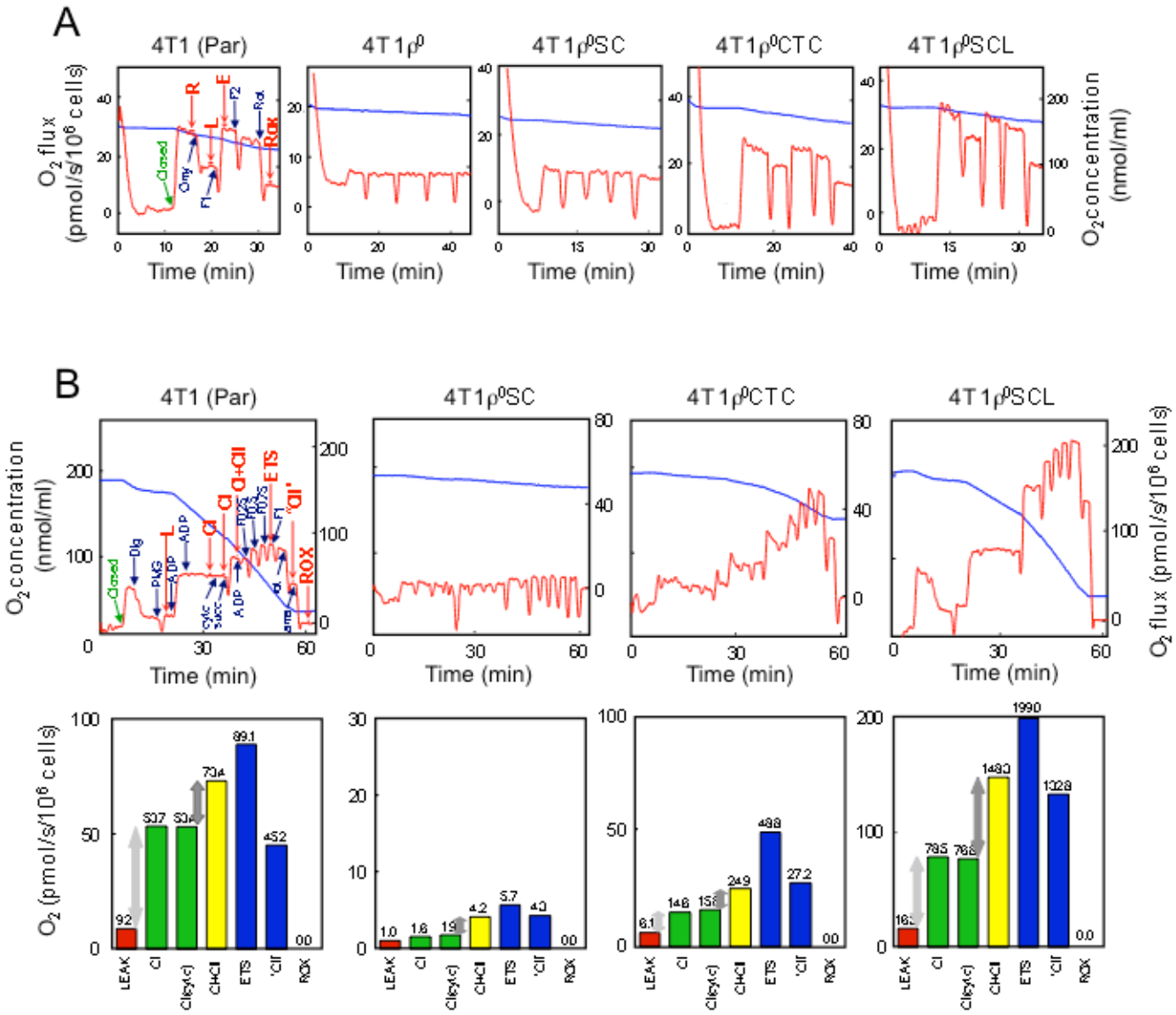
A
4T1 (Par)
4T1ρ0
4T1ρ0SC
4T1ρ0CTC
4T1ρ0SCL
O2 flux (pmol/s/10^6 cells)
O2 concentration (nmol/ml)
Time (min)
B
4T1 (Par)
4T1ρ0SC
4T1ρ0CTC
4T1ρ0SCL
O2 concentration (nmol/ml)
O2 flux (pmol/s/10^6 cells)
Time (min)
O2 (pmol/s/10^6 cells)
LEAK
CI
CI(ext.c)
CI+CII
ETS
'CII'
ROX

Supplementary Table I. Polymorphisms in 4T1 and B16 mtDNA confirm host origin of mtDNA in tumors derived from ρ^0 cells

Site	Base in Balb/c (reference*)	Base in 4T1ρ^0SC cells	Base in 4T1 cells	Gene
1574	T	T	C	*16S rRNA*
9829	A	A	-	*tRNA^{Arg}*
16076	A	A	G	*D-Loop*

Site	Base in C57BL/6 (reference*)	Base in B16ρ^0SC cells	Base in B16 cells	Gene
9821	- } 8A	- } 8A	A+ } >8A	*tRNA^{Arg}*
9829	-	-	-	*tRNA^{Arg}*
1035	C	C	T	*Nd4*

* see Bayona-Bafaluy e al 2003 and NC_005089.1